

POLITECNICO DI TORINO

Master's Degree in Aerospace Engineering

Master's Degree Thesis

Innovative ways of distribution for life-saving
medicines during emergency situations



Supervisors:

Enrico Cestino

Stefano Primatesta

Paola Crosasso

Corrado Calvo

Alessandro Perego

Candidate:

Francesco Cavallo

December 2020

This master's thesis has been realized in partnership with the hospital pharmacy service of *ASL Città di Torino*, Managing Director Dr. Crosasso Paola.

(Questa tesi magistrale è stata realizzata in collaborazione con il servizio di farmacia ospedaliera dell'ASL Città di Torino, Direttore Responsabile Dott.ssa Crosasso Paola)

Table of Contents

List of Figures	3
List of Tables.....	5
Abstract	6
Introduction	7
Literature Review	9
Research.....	12
Hospitals Research	12
UAVs Research.....	13
Multirotor.....	15
Fixed-Wing.....	15
Multirotor + Fixed-Wing.....	15
UAV Selection	18
Mission Definition	18
Hospital-to-Hospital	18
Hospital-to-Home	19
Principal Components Analysis (PCA).....	19
Overview of Statistical Learning.....	20
The importance of PCA	20
PCA Mechanism.....	21
PCA Result.....	24
Explained Variance.....	26
Matching	28
Regulatory Framework	30
EU Regulation	30
Italian Regulation	31
UAVs with a takeoff mass below 25 kg.....	31
UAVs with a takeoff mass over 25 kg	32
Airspace	32
Effects on the project	34
Simulation	35
Settings	35
Starting Point.....	35
Ending Point	37

Table of Contents

UAVs' features.....	39
Algorithm.....	40
Assumptions.....	40
Risk Map Layers	41
Hazardous Area	44
Risk Assessment	45
Layers Combination	48
Path Planning.....	49
Results.....	50
Risk Map and Trajectory (altitude 50 m).....	50
Fixed-wing.....	53
Small-size Multicopter	55
Mid-size Multicopter	58
Risk Map and Trajectory (altitude 20 m).....	60
3D Visualization	62
Above-the-River Solution.....	64
Comparison to Conventional Inter-Hospital Transportation.....	68
Conclusion.....	69
Bibliography	71
Appendix A – UAVs Data	76
Appendix B – Centro Anti Veleni	80
Appendix C – UAVs' PCA Scores	87

List of Figures

Figure 1 Map of major hospitals in Torino	12
Figure 2 UAV mass vs Endurance	16
Figure 3 UAV mass vs Cruise speed	16
Figure 4 Maximum payload mass vs Endurance	17
Figure 5 First two principal components loading vectors.....	24
Figure 6 First two principal components scores	26
Figure 7 Cumulative proportion of variance explained.....	27
Figure 8 First three principal components	28
Figure 9 Matching outcome.....	29
Figure 10 Altitude restrictions when flying close to airports	33
Figure 11 Map of the maximum allowed altitude in Torino area (17).....	34
Figure 12 Satellite view of Ospedale Molinette	35
Figure 13 Satellite view of the starting point (yellow area).....	36
Figure 14 In-site view of the starting point	37
Figure 15 Satellite view of Ospedale San Giovanni Bosco.....	37
Figure 16 Satellite view of the ending point (yellow area)	38
Figure 17 In-site view of the ending point	39
Figure 18 Simulation environment.....	41
Figure 19 Example of DJI Matrice 200's risk map.....	48
Figure 20 eBee X (on the left) and its risk map and optimum trajectory at 50 m of altitude (on the right)	53
Figure 21 WingtraOne (on the left) and its risk map and optimum trajectory at 50 m of altitude (on the right).....	54
Figure 22 Evo II (on the left) and its risk map and optimum trajectory at 50 m of altitude (on the right)	55
Figure 23 Mavic 2 (on the left) and its risk map and optimum trajectory at 50 m of altitude (on the right)	56
Figure 24 Phantom 4 RTK (on the left) and its risk map and optimum trajectory at 50 m of altitude (on the right)	57

List of Figures

Figure 25 Falcon x8 (on the left) and its risk map and optimum trajectory at 50 m of altitude (on the right) 58

Figure 26 Matrice 200 V2 (on the left) and its risk map and optimum trajectory at 50 m of altitude (on the right) 59

Figure 27 Phantom 4 RTK risk map and optimum trajectory at 20 m of altitude (left) and at 50 m of altitude (right).....61

Figure 28 Matrice 200 V2 risk map and optimum trajectory at 20 m of altitude (left) and at 50 m of altitude (right)..... 62

Figure 29 3D visualization of the simulation of the Matrice 200 V2..... 63

Figure 30 3D visualization of the simulation of the Phantom 4 RTK..... 63

Figure 31 Above-the-river trajectory 65

Figure 32 3D visualization of the above-the-river simulation of the Matrice 200 V2..... 67

List of Tables

Table 1 List of UAVs available on the market.....	14
Table 2 Matrix transcription of UAVs' data	21
Table 3 Loadings of the features on the first three principal components	25
Table 4 Sheltering Factor	43
Table 5 Simulation outcome at 50 m of altitude	51
Table 6 Total flight duration at 50 m of altitude.....	52
Table 7 Simulation outcome at 20 m of altitude	60
Table 8 Total flight duration at 20 m of altitude.....	61
Table 9 Above-the-river simulation outcome	66
Table 10 Above-the-river simulation - average risk and trajectory cost.....	66

Abstract

This master's thesis has the goal to provide effective research on the distribution of life-saving medications using UAVs. In partnership with *ASL Città di Torino* and *Città della Salute e della Scienza di Torino* represented by the doctors Corrado Calvo, Paola Crosasso, and Daniela Cestino, the project aims at the creation of a new procedure in order to faster the transportation of high priority drugs and blood derivatives. This aspect has already been highlighted in the literature (1; 2), proving drones could potentially overcome the logistic challenges as they are not subjected to traffic delays and they are able to reach regions that lack adequate roads faster.

In the first part of this thesis, the research has focused on hospitals' positions around the city of Torino. Then, several UAVs were identified to be analyzed. The research has been based on currently available mid-size drones in order to show the immediate possibility to turn this project into a real procedure in a small period of time. Also, another important aspect is the reliability of the system. Further on, the definition of different mission scenarios, together with *ASL Città di Torino*, led to a narrow selection of considered UAVs. This step has been done using Principal Components Analysis (PCA) method. This machine learning technique allows us to easily compare different features of the drones to select the most appropriate for a specific mission.

The second part of the thesis is focused on the delivery simulation from *Ospedale Molinette* to *Ospedale San Giovanni Bosco*. The calculation of the trajectory, thanks to the work of dr. Stefano Primatesta, take into consideration the possibility of a crash which could cause injuries and damages. Also, a regulatory section is addressed, relying on the Italian regulator, *Ente Nazionale per l'Aviazione Civile* (ENAC). In particular, flying restrictions above highly populated urban areas are taken into consideration and could limit the application of this solution.

Introduction

At the beginning of 2020, the world faced a new kind of pandemic which caught everyone unprepared. Many lockdowns have been deployed in order to prevent the spreading of the Covid-19 virus. Moreover, the lack of personal protection equipment (PPE) in the first stages of the crisis and the high transmissibility of this coronavirus have shown how avoiding people to move from a place to another is important.

During emergency situations, a hospital could not have enough equipment or medications to overcome the emergency. Until now, a conventional vehicle from another hospital or warehouse is deployed to deliver what is needed. That means a driver and a van are required to complete this task. Moreover, the delivery time depends on the traffic of the city, which means it could take a considerable amount of time, especially in an emergency, in which people try to reach hospitals for treatments or look for relatives and friends. Therefore, a new scheme to assure the transportation could take place quickly and safely is required.

A worldwide growing market could be the answer to the problem. Indeed, Unmanned Aerial Vehicles (UAV) have the potential to overcome current difficulties. In Italy alone, the market value for this sector was around 100 million euros in 2018. That comprises more than 700 companies, divided into hardware manufacturers, software developers, and services providers for third part companies utilizing their own drones or renting ones (3). Therefore, the high potential and the growing capabilities of UAVs led to the identification of this sector as the most promising one for this project.

Since the early stage of applications of this technology, 77% of companies in this market report investments in Research and Development. Furthermore, concerning UAVs experimentations, three main clusters emerge, namely security surveillance (56%), inspections for utilities (26%), and logistics (18%) (3). Hence, there is great research to run operations with UAVs more safely and efficiently.

Looking at the European area, almost 200 companies produce and deliver UAVs to the market (4). Therefore, a high number of different drones are available, which makes difficult a selection among them. To not be overwhelmed by all this information, some algorithms have been developed to select the best drone to run an operation (5). Also, a different approach, by using statistical learning methods, can be found later on in this thesis.

Introduction

Since this market is quickly growing, and its applications involve every sector, the regulatory authorities are following its development. This industry is becoming highly regulated to control the increasing number of drones in circulation. Regulations represent the hardest aspect to overcome because of the urban nature of this project. Indeed, drones and the operation itself must respect some requirements on instrumentation and trajectory of the flight. Since the first one depends on the UAV only, this work is focused mainly on the second, by proving a method to better address the requirements on flying over critical areas.

Literature Review

In the healthcare sector, drones have shown great potential in the delivery of medicines or blood products. Moreover, they are considered a valuable solution to overcome logistic challenges since they are not affected by traffic delays and can reach isolated areas that lack adequate roads quicker. However, they could be utilized only when the quality of transported products is not adversely affected. In the literature, it is possible to find several case studies that address the use of UAVs in healthcare.

A general study conducted by Thiels et al. (2) provides a useful insight into the application of drones in healthcare. Their work put an emphasis on the different kinds of hospitals in the US. Indeed, the fact that a large number of Americans have not quick access to a trauma center brings them to go to smaller hospitals, which have limited resources. Hence, the work shows that this problem could be addressed by UAVs, which can quickly deliver medicines and blood products from larger hospitals to smaller ones. Moreover, it avoids the transportation of the patient towards more equipped centers, which is usually expensive, and it may delay the adequate initial treatment.

Focusing on the quality of the transportation, Hii, Courtney, and Royall's work (1) shows the effects of temperature and vibration of a drone flight on insulin. They chose this medicine because of its sensitiveness to environmental stresses. Indeed, this peptide-based drug easily unfolds to cause irreversible aggregation when subjected to high temperatures and exposure to vibration or agitation. Alteration of the structure of insulin will result in an impairment of its biological efficacy.

The result of the study proved that insulin quality was maintained after exposure to environmental stresses that simulate a 30-minute UAV delivery, which involves temperatures from -20°C to $+40^{\circ}\text{C}$ and vibration frequencies in the range of 0–40 Hz).

Following the quality requirements of transportation, the work produced by Amukele et al. (6) aims to demonstrate the safety of the delivery of blood products using drones. The study regards red blood cells (RBCs), platelets (PLTs), and plasma units frozen within 24 hours of collection (FP24). Different types of UAVs, multicopter of fixed-wing, have been used. Moreover, since blood products for the purpose of transfusion are not subjected to stringent IATA regulation of infectious substances, the approach for packing followed by (6) was to mimic methods used for road transportation of blood products while

minimizing the number of passive temperature buffers, due to payload constraints.

The result of the analysis proved that the transportation of RBCs, PLTs, and FP24 units using UAVs has no adverse consequences. In particular, the authors were concerned about the temperature and the acceleration to which blood products were exposed. They overcame the first problem by using coolers used for in-hospital transportation of these products. For the second issue, they selected the multicopter category of drones for undergoing significantly less acceleration and deceleration and guaranteeing an accurate takeoff and landing.

Conversely, the work conducted by Eichleay et al. (7) provides a wider view of the benefits and risks of using drones in the healthcare sector. This study highlights the complexity brought by adding new systems, such as UAVs, to the already complex healthcare environment. In particular, companies that work with the delivery of medical goods must be prepared to implement this technology into their systems. Moreover, health professionals must undergo specific training to effectively run operations involving drones. Hence, adding UAVs to the health system could have an impact on the health workforce.

Concerning the hospitals and medical warehouses, (7) highlights how their logistic systems must be updated to welcome the inclusion of UAVs. Indeed, optimizing routing will require a new set of variables to determine the most efficient route. Furthermore, the financial assessment must be taken into account because it may represent a possible barrier to some applications of UAVs in healthcare. In fact, using them implies a tradeoff between weight, distance, and cost. For this reason, transportation using drones will likely supplement medical supply chains, rather than replace road transport. Moreover, this study shows how crucial and complex is to understand under which conditions drones are cost-effective. Lastly, an insight into the critical role played by the governance in regulating air space and the transportation of medical goods through drones is reported.

The analysis, realized by Eichleay et al. (7), also provides a UAV Delivery Decision Tool that aims to help the user to overcome all the issues written above. Users start defining the transport problem they are trying to solve using UAVs. Then, they insert transportation parameters. The last part regards offline worksheets to select and analyze stakeholders and the identification of preliminary sites for UAV operations.

The literature review has shown how important the implementation of UAVs is in the healthcare sector. Universities, hospitals, and private companies are investing in this new technology to find new and innovative ways to implement

them. Although the relatively new interest in them, large corporations are already starting to use them for their delivery purposes (8). Therefore, the transportation of medicines, blood products, or biological samples using UAVs is already part of the present. Since the research has proved that this kind of delivery has no adverse consequence on transported goods, more and more drones are likely expected to fly for medical purposes.

Research

The first step of the research for this master's thesis regards the hospitals in Torino. This part was crucial to determine the distances among them, allowing further planning for medication storage. The second part consists of the research of commercial UAVs suitable for this application. Small drones and heavy cargo ones were discarded, due to payload and regulatory restrictions.

Hospitals Research

Using any GPS data provider, such as Google Maps (9), it is possible to know the exact position of each hospital in the metropolitan area of the city of Torino. Once the geographical coordinates are collected and the map is set, it is possible to have an overview of hospital distribution in the urban area of Torino.



Figure 1 Map of major hospitals in Torino

The result is visible in Figure 1. Only hospitals with emergency rooms were considered. Other clinics were discarded because the project focuses on emergency situations. Indeed, on those occasions, people who suffered injuries are redirected to major hospitals for better emergency care.

Two main hospitals were chosen, one for each main Local Health Units in Torino: *Ospedale Molinette* for *AOU Città della Salute e delle Scienze* and *Ospedale San Giovanni Bosco* for *ASL Città di Torino*. These two hospitals, positioned at the opposite sides of the city, represent the perfect case for the application of a new extra-hospital transportation system. Moreover, this step is crucial to calculate straight-line distances among all health centers in Figure 1 to have a first idea of the range to be covered. Later on in this thesis, details about these two hospitals will be discussed in the simulation section.

UAVs Research

Willing to provide a solution quickly ready, only UAVs currently available on the market were considered. Experimental drones built inside universities, for example, were excluded due to assembly complications and larger delivery time compared to mass-produced ones. Moreover, small drones and heavy cargo ones were discarded, due to payload and regulatory restrictions. Therefore, the research took place on the websites of manufacturers and online dealers. A total number of 38 UAVs were found. In Appendix A, a table reports all available data for each of them.

Manufacturer	Name
Airborne Drones	Falcon x4
	Falcon x8
	Vanguard
Autel Drones	Evo II
DJI	Inspire 2
	Matrice 200 V2
	Matrice 600
	Mavic 2
	MG-1P
Ewatt Aerospace	Phantom 4 RTK
	ESPECT
	EWG-E3
	EWZ-D6

Manufacturer	Name
	EWZ-S8
Freefly	Alta 8 Alta X
Intel	Drone Intel® Falcon™ 8+
	BIGONE 8HSE EVO4HSE RTK
Italdron	Levante Titan LE Titan XLE
Matternet Inc.	M2V9
Nextech	ATLAS-T ATLAS-V
senseFly	eBee SQ eBee X
Skyrobotic	SF6 VTOL RPV
UAV System int.	Tarot 650
UAVOS	UVM 2E
Valkyrie	Heavy Pro
Vertical Technologies	DeltaQuad Pro #CARGO
VideoDrone Finalnd Oy	Videodrone
Wingtra	WingtraOne
xFold	Cinema Serie
	H520
Yuneec	Tornado H920 Typhoon H3

Table 1 List of UAVs available on the market

All the drones above were analyzed and they could be divided into three main clusters:

- Multirotor;
- Fixed-Wing;
- Multirotor + Fixed-Wing.

Multirotor

The drones analyzed have from four to eight rotors, depending on the size of the aircraft. This kind of UAV is capable to perform a vertical takeoff and landing. Moreover, this cluster represents the majority of the UAVs analyzed. In general, they are agile, but the top speed reached is the lowest among the three categories. Also, the average maximum flight time deeply depends on the flight speed and it is consistently lower than the other two clusters.

Fixed-Wing

This type of UAV permits high range and endurance, thanks to the lift generated by the wing. It is usually normal to come across this kind of aircraft in the military for surveillance purposes. For civilian applications, they are usually smaller and used for mapping large areas, but their cost is sensibly higher than a comparable multirotor drone. Indeed, there are few available mid-size UAVs of this kind. The reason could also lie in the need for an adequate area for takeoff and landing.

Multirotor + Fixed-Wing

This particular kind of aircraft put the qualities of the other two together. These UAVs could perform a vertical takeoff and landing, moreover, their maximum flight time is higher than the first cluster, thanks to the lift provided by the wing.

In general, it is possible to highlight different UAV features by comparing some of their characteristics. Indeed, common behaviors emerge, as can be seen in the graphs below, in which every blue dot represents a drone. Moreover, a red trend line is added to better understand the average relationship between two attributes.

In the first plot, the link between the weight of UAVs and their endurance is shown. The endurance slightly increases as the weight of the drones increases. The explanation of this phenomenon lies in the larger batteries usually carried in bigger UAVs. Also, some of the drones have a highly above-average

endurance, thanks to the fact they are a wing-type system. Indeed, that system allows larger flight times at the cost of larger overall dimensions of the drone.

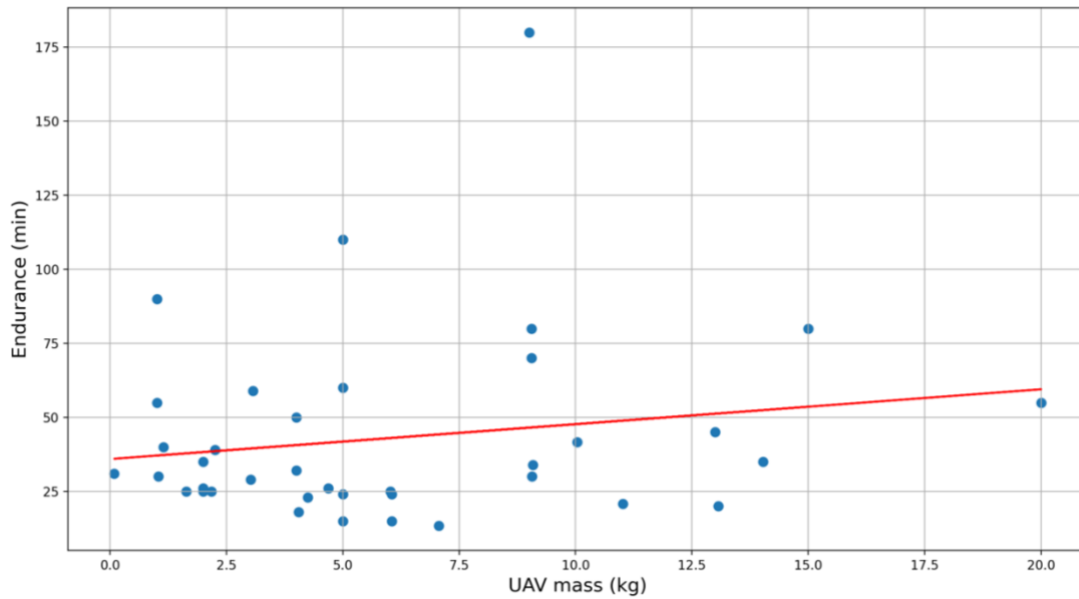


Figure 2 UAV mass vs Endurance

In the following graph, another important relation, involving drones' masses, is highlighted. Looking at the cruise speed for different UAVs, it is clear it decreases for heavier drones. Indeed, lightweight drones allow higher cruise speeds; hence they could have a critical role in this project, in which the velocity is crucial in delivery during emergencies.

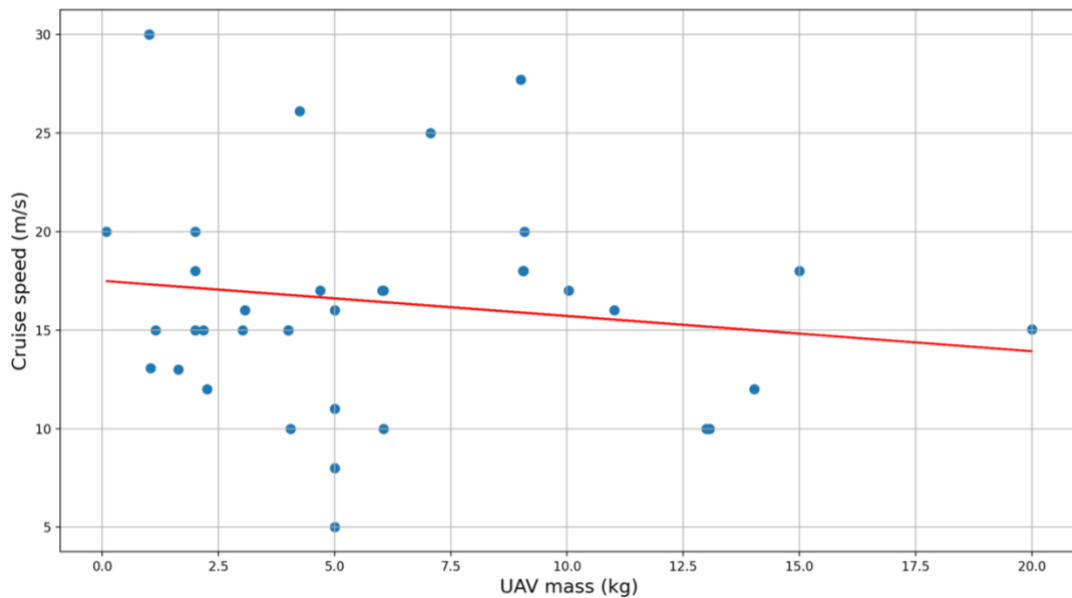


Figure 3 UAV mass vs Cruise speed

The last graph wants to show the relation between the maximum transportable payload weight and endurance. The result is a decreasing max flight time as the

payload mass rises. This behavior is in contrast with the one in Figure 2. It could be explained considering that a high-endurance drone needs to carry considerable weight in batteries, leaving out the payload.

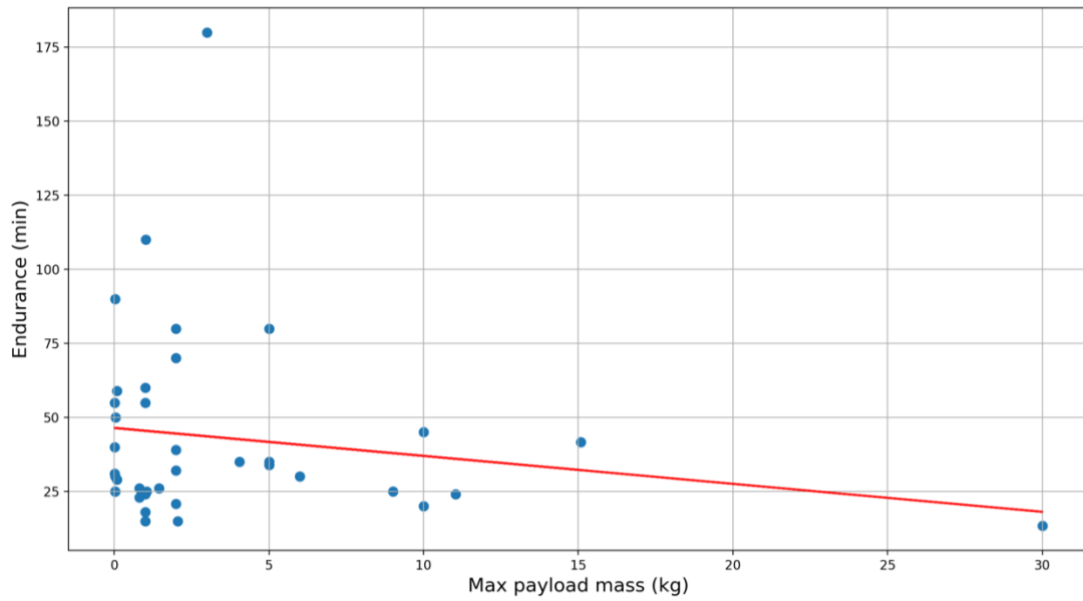


Figure 4 Maximum payload mass vs Endurance

UAV Selection

In this chapter, a screening of all UAVs analyzed will be performed, based on the mission requirements discussed together with doctors Corrado Calvo, Paola Crosasso, and Daniela Cestino from both local health units *ASL Città di Torino* and *Città della Salute e della Scienza di Torino*. Indeed, the first part of this section involves the definition of the missions desired while the second focuses on assigning certain drones to a specific mission. For this second part, a machine learning algorithm, called Principal Components Analysis (PCA) will be to catalog UAVs.

Mission Definition

The definition of a mission is a crucial step to select the best drones to complete it. Not all the UAVs are the right choices for a specific mission. Indeed, considering the previous chapter, a drone's features depend on multiple factors, such as its type (multirotor, fixed-wing, or multirotor + fixed-wing) or overall dimensions.

Listening to the needs and requirements of both local health units involved in this project, two categories of missions were identified: Hospital-to-Hospital transportation and Hospital-to-Home transportation. In the following pages, a better explanation of every mission pinpointed is provided.

Hospital-to-Hospital

In this scenario, there is a need for a new transportation system between hospitals during emergencies. It is the easiest to implement, regarding the regulatory framework and the route definition. Indeed, in the case of only two hospitals considered, the same route could be used at every flight, optimizing delivery time and risk. The first of the two missions identified regards the transportation of medicines while the second one the transportation of biological samples. They have some aspects in common, but they differ in the regulatory part. In particular, the two missions have the following requirements.

Medicines

Medicines need to be given to the patient in a short time after the diagnosis. Antidotes with priority 1, which must be used within 30 minutes (more information follows in Appendix B) and antidoted with priority 2, which must be used within 2 hours, are the drugs selected for this mission. They also

require specific temperature conditions, depending on the antidote. Moreover, every drug is stored in a particular container, which means that this aspect must be taken into consideration to deal with constraints in terms of payload mass and volume.

Biological Samples

Biological samples also require specific temperature conditions, and their mass and volume must be checked to not be a limitation for the flight. On the other hand, transportation must respect the regulation for this category. Indeed, it is critical to guarantee a safe delivery from a hospital to another.

Hospital-to-Home

This other scenario represents a more complicated challenge compared to the previous one. This category comprises the transportation of items from a hospital to any other location, such as buildings, parks, or the site of an accident. The goods mentioned are the same as the Hospital-to-Hospital scenario, with an oxygen tank in addition. Whilst this new component does not have to comply with a specific sanitary regulation for transportation, it does have to for the UAV regulation. Indeed, an oxygen tank has a significant weight and volume that could represent an enormous limitation for flight.

In addition, the fact of repeatedly changing the route of the delivery represents an obstacle due to ENAC regulation (10). Indeed, every route requires approval from *Ente Nazionale per l'Assistenza al Volo* (ENAV), the Italian air traffic controller. That means direct communication with this entity is required, with the risk of delays for the mission to be completed. A better understanding of the regulatory framework is provided in the next chapter. For the reasons explained above, the Hospital-to-Home scenario will not be considered for this project, due to its complications. Indeed, only the Hospital-to-Hospital one has the right characteristics to be implemented in a short time. Nonetheless, further developments must include this scenario to provide people with better health care.

Principal Components Analysis (PCA)

Before going deeper into PCA, a better explanation of machine learning techniques is provided. In particular, for this thesis, the statistical learning field has been explored. To this purpose, the book “An Introduction to Statistical Learning: with Applications in R (11)” has been helpful to understand this field of study and to apply its techniques to this master’s thesis.

Overview of Statistical Learning

Statistical learning refers to a vast set of tools for understanding data. These tools can be clustered in supervised or unsupervised. Generally speaking, supervised statistical learning techniques involve building a statistical model for predicting, or estimating, an output based on one or more inputs. Moreover, the output can be verified through methods that can measure the quality of the results obtained. Problems of this nature occur in fields as diverse as astrophysics, business, public policy, and medicine.

On the other hand, with unsupervised statistical learning, there are inputs but no supervising output; nevertheless, we can learn relationships and structure from such data. It is more challenging, because the utilization tends to be more subjective, and there is no simple goal for the analysis, such as prediction of response. Unsupervised learning is often performed as part of an exploratory data analysis. Indeed, in this thesis, it will be used to give meaning and cluster data from UAVs.

The importance of PCA

Delving into the PCA method, it is a type of unsupervised learning that is a popular approach for deriving a low-dimensional set of features from a large set of variables. To start the analysis, it is crucial to explain that there is a need for lowering the number of variables.

Taking into consideration UAVs data used for this analysis, some of them could be found in Appendix A, it is clear that the number of the features is too large to expect to manage to have all of them in a single graph and get an understandable result. In particular, these features are:

- Endurance;
- Range;
- Weight;
- Width;
- Length;
- Height;
- Maximum payload weight;
- Cruise speed;

- Max wind resistance;
- Price.

The goal is, indeed, to visualize $n=38$ observations¹ with measures on a set of these $p=10$ features. It is possible to perform this analysis by examining two-dimensional scatterplots of the data, each of which contains the $n=38$ observations' measures on two of the features. Calculating the number of plots required to do this, let's take the number of features considered. The result of the combination is $\binom{p}{2} = p(p - 1)/2$. In his case, in which $p=10$, the total number of two-dimensional scatterplots required is 45. Hence, it would be helpful to find a low-dimensional representation of the data that captures as much of the information as possible.

PCA Mechanism

To better understand the mechanism behind PCA, it is useful consider the $n=38$ UAVs and their $p=10$ features each as a matrix. Indeed, every row corresponds to a drone, or observation, while every column represents their features, or dimensions. In mathematical language, it means that each of the n observations lives in a p -dimensional space. This drones' dataset now takes the name of X and the index used for the rows is $i = 1, 2, \dots, n$, while the one used for the columns is $j = 1, 2, \dots, p$. The crucial part is that not all of these dimensions are evenly "interesting". In particular, the concept of "interesting" is measured by the amount that the observations vary along each dimension.

	Feature 1	Feature 2	Feature j	Feature p
UAV 1	x_{11}	x_{12}	x_{1j}	x_{1p}
UAV 2	x_{21}	x_{22}	x_{2j}	x_{2p}
UAV i	x_{i1}	x_{i2}	x_{ij}	x_{ip}
UAV n	x_{n1}	x_{n2}	x_{nj}	x_{np}

Table 2 Matrix transcription of UAVs' data

PCA seeks a small number of dimensions that are as interesting as possible. Each of the dimensions found by PCA, which now can be called principal components, is a linear combination of the p features. In order to be clear on

¹ The number of drones analyzed. More information is available in Appendix A.

the notation used, it is important to clarify how a feature will be written in the following passages. For instance, the first feature will be

$$X_1 = \{x_{11}, x_{21}, \dots, x_{n1}\}$$

Going into detail with the calculus, the first principal component of a set of features X_1, X_2, \dots, X_p is the normalized linear combination of the features

$$Z_1 = \phi_{11}X_1 + \phi_{21}X_2 + \dots + \phi_{p1}X_p$$

that has the largest variance. “Normalized” means that $\sum_{j=1}^p \phi_{j1}^2 = 1$. Moreover, the elements $\phi_{11}, \phi_{21}, \dots, \phi_{p1}$ are called the loadings of the first principal component. Consequentially, the loadings form the principal component loading vector $\phi_1 = (\phi_{11} \ \phi_{21} \ \dots \ \phi_{p1})^T$. The constraint on the sum of the square of the loadings equal to one is crucial, since otherwise setting these elements to be arbitrarily large, in absolute value, could result in an arbitrarily large variance.

Since only the variance has relevance, it is reasonable to standardize each of the variables in \mathbf{X} to have mean zero, which means that the column means of \mathbf{X} are zero. Indeed, it means a simple scaling to set the mean value of each column is required before moving forward. Processing one row at the time and applying the same principles as before, it is required to find the linear combination of the feature values of the form

$$z_{i1} = \phi_{11}x_{i1} + \phi_{21}x_{i2} + \dots + \phi_{p1}x_{ip}$$

that has the largest variance, respecting the constraint of $\sum_{j=1}^p \phi_{j1}^2 = 1$. In other terms, the first principal component loading vector solves the optimization problem

$$\max_{\phi_{11}, \dots, \phi_{p1}} \left\{ \frac{1}{n} \sum_{i=1}^n \left(\sum_{j=1}^p \phi_{j1} x_{ij} \right)^2 \right\} \quad \text{subject to} \quad \sum_{j=1}^p \phi_{j1}^2 = 1$$

It is the same as writing

$$\max_{\phi_{11}, \dots, \phi_{p1}} \left\{ \frac{1}{n} \sum_{i=1}^n z_{i1}^2 \right\}$$

$z_{11}, z_{21}, \dots, z_{n1}$ are called the scores of the first principal component and, since the average value for each feature (or column) was set to zero, which means $\frac{1}{n} \sum_{i=1}^n x_{ij} = 0$, scores' average is also zero. Therefore, the objective to maximize

is just the sample variance of n values of z_{i1} . This problem could be solved through an eigen decomposition.

Another significant aspect of the first principal component is yet to be highlighted. Indeed, an interesting geometric interpretation of it could be done. Considering the p -dimensional space generated by the features, where each of the observations x_{ij} lives in, the loading vector $\phi_1 = (\phi_{11} \ \phi_{21} \ \dots \ \phi_{p1})^T$ defines a direction in this space along which the data vary the most. If we project the n data points x_1, x_2, \dots, x_n onto this direction, the projected values are the principal component scores $z_{11}, z_{21}, \dots, z_{n1}$ themselves.

The focus has been on the first principal component Z_1 so far, but the analysis now can move on to the second principal component Z_2 . As Z_1 , the second principal component is a linear combination of X_1, X_2, \dots, X_p that has maximal variance out of all linear combinations that are uncorrelated with Z_1 . Repeating the same process as before, the second principal component scores $z_{12}, z_{22}, \dots, z_{n2}$ are calculated through the expression

$$z_{i2} = \phi_{12}x_{i1} + \phi_{22}x_{i2} + \dots + \phi_{p2}x_{ip}$$

in which $\phi_2 = (\phi_{12} \ \phi_{22} \ \dots \ \phi_{p2})^T$ is the second principal component loading vector. Recalling the uncorrelation required between Z_1 and Z_2 , it means imposing the constraint that the direction ϕ_2 must be orthogonal to the direction ϕ_1 . Thus, a similar optimization problem to the previous case needs to be solved to find the second principal component loading vector. Indeed, it is

$$\max_{\phi_{12}, \dots, \phi_{p2}} \left\{ \frac{1}{n} \sum_{i=1}^n \left(\sum_{j=1}^p \phi_{j2} x_{ij} \right)^2 \right\} \quad \text{subject to} \quad \sum_{j=1}^p \phi_{j2}^2 = 1 \quad \text{and} \quad \langle \phi_1, \phi_2 \rangle = 0$$

and differs from the previous optimization problem by the constraint of orthogonality between ϕ_1 and ϕ_2 , which is represented by their scalar product equals to zero.

Once this mechanism is doubtless, it is possible to create higher orders of principal components Z_j , by merely repeating the same process. Nevertheless, these principal components must always be uncorrelated to their previous ones, which again is translated by constraining their loading vectors to be orthogonal to each other. Then, a comparison among different principal components, for instance, Z_1 and Z_2 , or Z_1 and Z_3 , or Z_2 and Z_3 , could be executed.

PCA results are usually shown with the help of a biplot display. This type of chart allows us to represent both the principal component scores and the loading vectors. Visual examples are provided below once the PCA is used on the UAVs' database.

PCA Result

Applying the mechanism explained above in a Python (12) environment with the help of the "scikit-learn" library (13), a PCA analysis of the UAVs' data set has been performed. The result is shown in the image below.

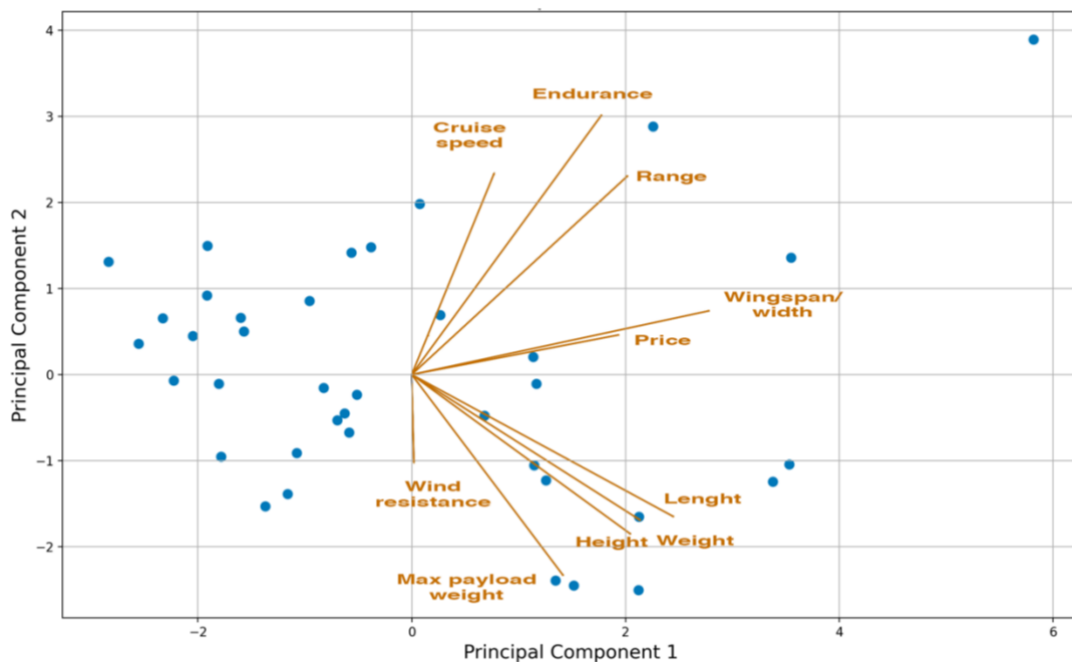


Figure 5 First two principal components loading vectors

In Figure 5, it is possible to see the first two principal components loading vectors. Every blue dot represents a drone, or observation as it was named in the explanation, and shows its score for the first two principal components. Recalling what has been written on the PCA method, it is a part of the unsupervised statistical learning used as an exploratory analysis. Hence, this case refers to that use. Looking at the loading vectors in Figure 5, it is possible to say that the first principal component, the x-axis, represents a sort of overall dimension and price of the UAVs. Indeed, the loadings for these two features on the first principal component are predominant in respect of their loadings on the second principal component. Therefore, this analysis makes the x-axis a measure of the dimensions and price.

On the other hand, the second principal component, the y-axis, represents a balance of the drones' performances. Indeed, the loadings, such as Cruise speed, Endurance, Range, Wind resistance, and Maximum payload weight,

have a larger portion on the second principal component compared to the portion on the first principal component. Moreover, looking at Figure 5, it is evident that several loading vectors are closer than others. This characteristic means that the features represented by close loading vectors are somehow correlated. This correlation is observable in the Cruise speed, Endurance, and Range cluster in the top right of the chart or Length, Weight, Height, and Maximum payload weight cluster in the lower part of the graph.

In Table 3, the list of all the loadings on the first three principal components can be found.

	Principal Component 1	Principal Component 2	Principal Component 3
Endurance	1,77	3,01	-1,19
Range	2,02	2,31	0,45
Weight	2,13	-1,69	-0,50
Width	2,78	0,74	0,20
Length	2,45	-1,65	0,71
Height	2,04	-1,85	-0,64
Max payload weight	1,41	-2,33	2,68
Cruise speed	0,77	2,33	1,85
Wind resistance	0,02	-1,01	-4,32
Price	1,93	0,46	-1,99

Table 3 Loadings of the features on the first three principal components

Those values have been multiplied by six compared to the values obtained with the PCA algorithm. This operation does not affect the result, but it has been made for graphic reasons. In this way, the directions of the loading vectors,

which carry all the information needed, are more visible. In fact, the magnitude of these loadings is not relevant for this application.

Hence, it is possible to divide the chart in Figure 5 into four areas:

- **Top left.** They are small UAVs with higher cruise speed and endurance, and considerable range;
- **Top right.** They are large UAVs with higher cruise speed and endurance, and considerable range;
- **Bottom left.** They are small but heavier UAVs with lower cruise speed, better wind resistance, and larger payload capability;
- **Bottom right.** They are larger and heavier UAVs with lower cruise speed, better wind resistance, and larger payload capability.

The scores of each drone are reported in Appendix C, while the whole picture is available in Figure 6. Their position in the chart shows in which category a drone is.

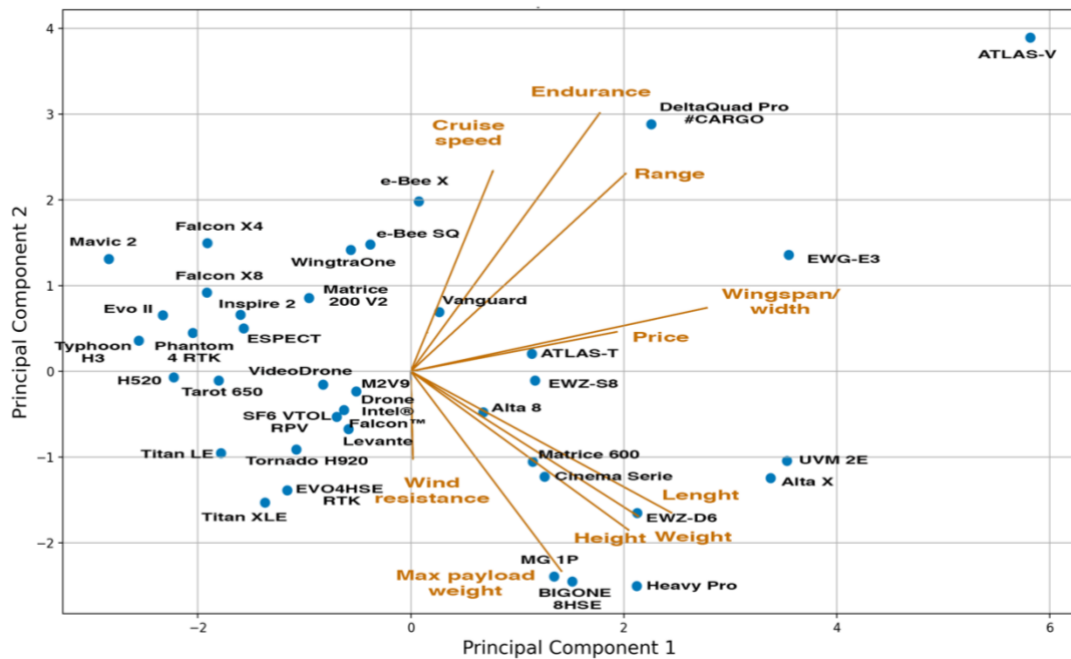


Figure 6 First two principal components scores

Explained Variance

Before matching the mission requirements with the specifics of the drones, a comment on the outcome of the PCA is required. Converting a p -dimensional space into a lower-dimensional space means some of the information (variance) carried in the data is lost. Therefore, the interest is now finding the

proportion of variance explained by each principal component. Assuming the variables have been centered to have mean zero, the total variance present in a data set is defined as

$$\sum_{j=1}^p \text{Var}(X_j) = \sum_{j=1}^p \frac{1}{n} \sum_{i=1}^n x_{ij}^2$$

while the variance explained by the m -th principal component is given by

$$\frac{1}{n} \sum_{i=1}^n z_{im}^2 = \frac{1}{n} \sum_{i=1}^n \left(\sum_{j=1}^p \phi_{jm} x_{ij} \right)^2$$

Thus, the proportion of variance explained by m -th principal component is obtained as

$$\frac{\sum_{i=1}^n \left(\sum_{j=1}^p \phi_{jm} x_{ij} \right)^2}{\sum_{j=1}^p \sum_{i=1}^n x_{ij}^2}$$

In Figure 7 the cumulative proportion of variance explained is shown.

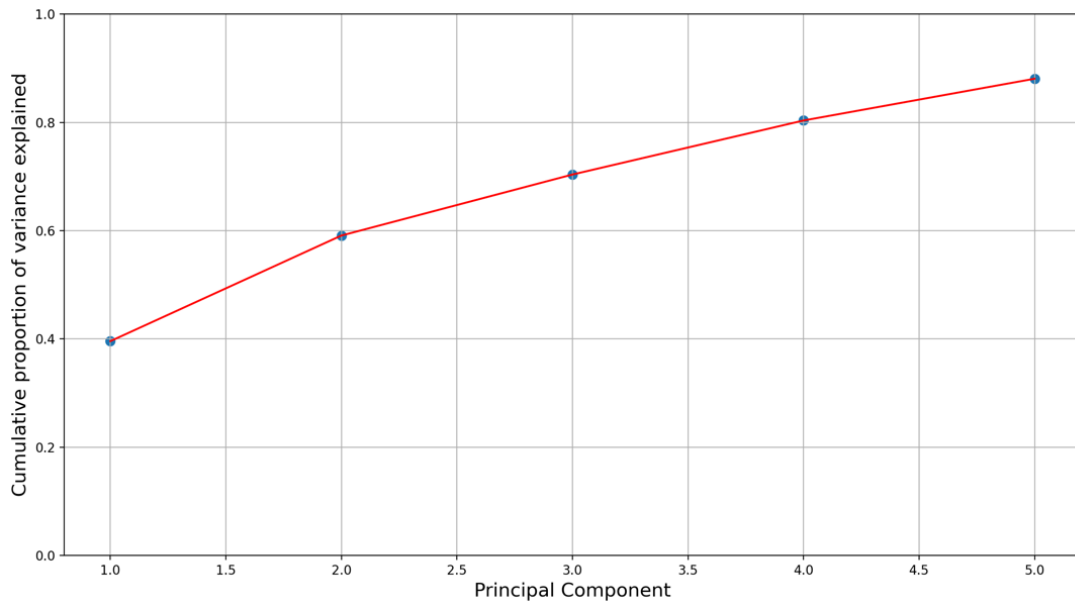


Figure 7 Cumulative proportion of variance explained

This chart shows the first two principal components explain almost 60% of the variance of the data. Hence, some of the information has been lost. A solution could be rising the number of principal components used, with the risk of complicating the interpretation of the outcome. In Figure 8, the result using three principal components is reported. Using more than three principal components leads to a difficult graphic representation.

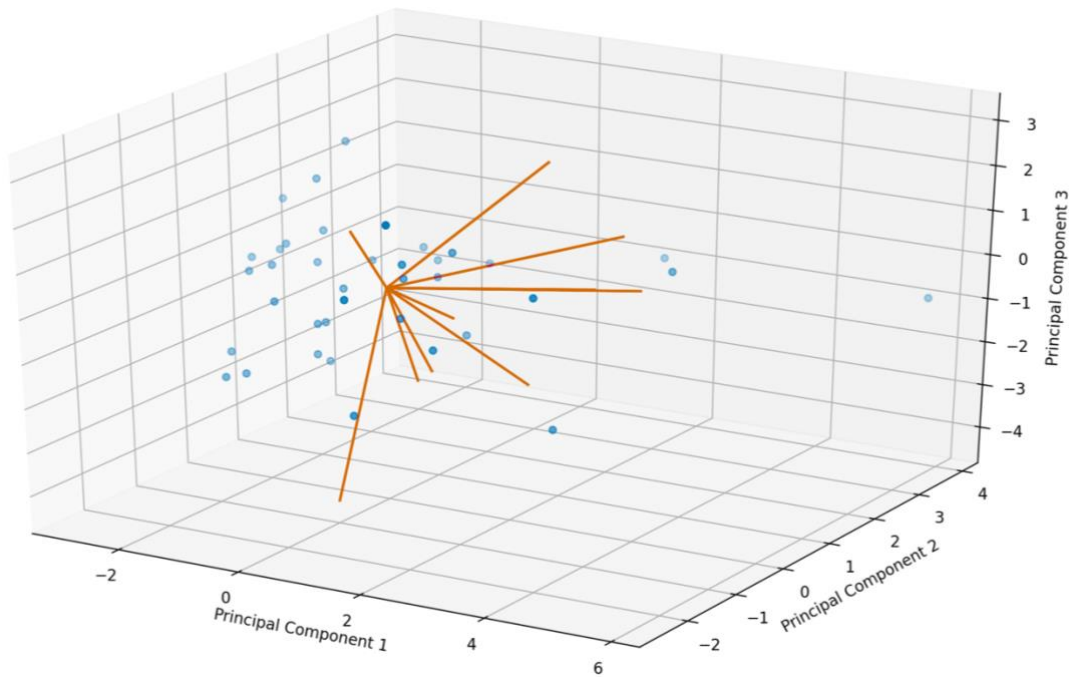


Figure 8 First three principal components

Adding a third principal component (and dimension) to the analysis brings more accuracy. Indeed, the first three principal components explain 70% of the variance of the data. However, this 10% more information carries the complication of dealing with high-dimensional charts. Moreover, the last principal component added is a sort of balance of the drones' performances too. Therefore, although some of the information is lost in the process, using only the first two principal components is preferred, as long as they help to visualize and interpret the data.

Matching

At the beginning of this chapter, a series of missions were defined. In particular, the focus has been on the Hospital-to-Hospital category, thanks to a more conducive regulatory framework. Hence, the two missions identified were the transportation of medicines, such as antidotes, and biological samples. Since the lowest possible delivery time and the low payload required are shared requisites, the same drone could accomplish this kind of mission.

Once the mission requirements are set, the matching procedure could be completed looking at Figure 6. Indeed, the lowest possible delivery time means that the cruise speed must be as large as possible. Therefore, the analysis revolves around the upper part of the chart. However, in a hospital environment during an emergency, smaller UAVs are preferred. Indeed, smaller drones usually required shorter times to be ready to fly and could be stored almost everywhere without any restrictions due to their size. This last

consideration shifts the area of interest on the top left of the graph. The UAVs there are the chosen ones to perform the simulation. Moreover, the city of Torino has an average wind velocity of around 7 km/h (≈ 2 m/s) throughout the year with a peak of 102 km/h ($\approx 28,4$ m/s) in 2013 (14). Hence, all the drones resist the average wind while none of them could fly in the maximum wind velocity condition.

In Figure 9, the outcome of matching is shown. The red dots in the top left of the chart represent the drones ultimately selected.

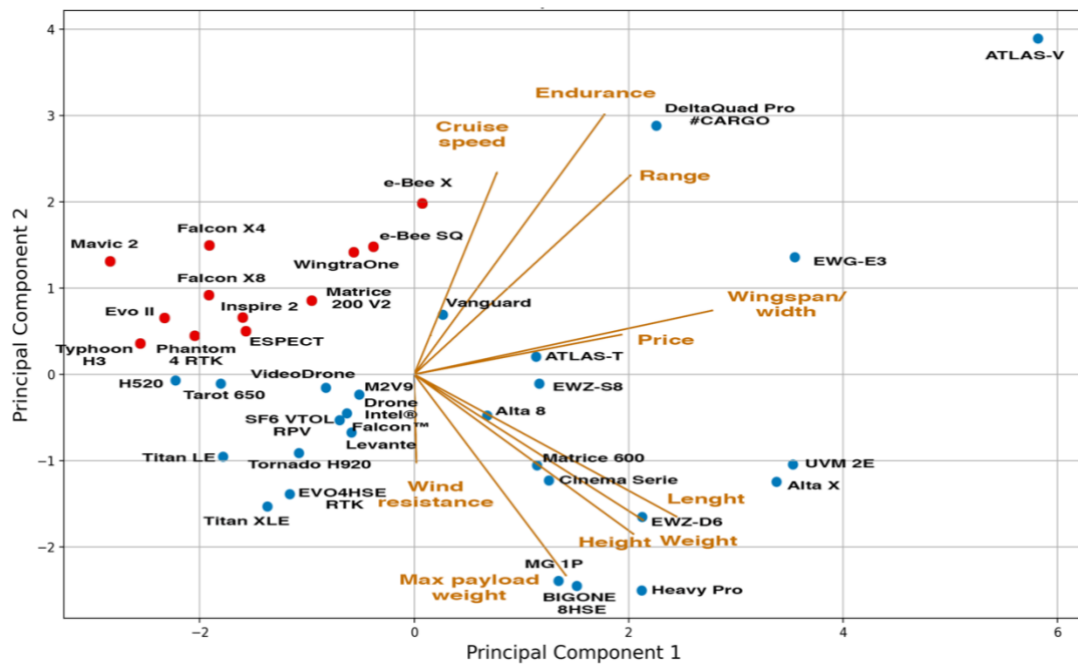


Figure 9 Matching outcome

Regulatory Framework

The UAV market is continuously growing with new players and applications every day. As a consequence, the regulatory authorities must keep the regulations and procedures up to date. Since this project is designed for an application in Italy, the reference authority is ENAC.

The first edition of the Italian UAV Regulation (*Regolamento Mezzi Aerei a Pilotaggio Remoto*) was published in December 2013, by implementing article 743 of the Italian Navigation Code (*Codice della Navigazione*), which identifies UAVs as aircraft and establishes that ENAC must cover the regulatory framework. After this first edition, continuous updates were published in order to keep track of the evolution of the market. Aiming to standardize the regulatory framework across the European Union, in June 2019, the European Commission (EC) released two EC Regulations. The first is Delegated Regulation 2019/94516 (15), which enshrines the rules for UAV marketing. The latter is Implementing Regulation 2019/94717 (16), which establishes the norms for operations, pilots, and operators. In response to those EC Regulations and with the purpose of driving the transition of this sector from the national regulation to the European one, in November 2019, ENAC published the third edition of the Italian UAV regulation, which brings the national requirements towards the European ones. Moreover, in July 2020, a further update (10) of the third edition, which is used as a reference in this master's thesis, was released.

EU Regulation

Conversely to previous editions, in (15; 16), there is no more distinction between professional and recreational uses. In fact, the differentiation is based on the level of risk of the operation, which is evaluated with the SORA (Specific Operations Risk Assessment) methodology issued by JARUS (Joint Authorities for Rulemaking on Unmanned Systems). Therefore, the EU Regulation defines three classes of operations, namely Open, Specific, and Certified.

Open (A)

UAV operations in the “open” category are not subject to any prior authorization or to a declaration of the operation before it takes place. The UAVs must respect a series of requirements, such as a maximum takeoff mass of 25 kg, a maximum flight altitude of 120 m, and keeping the aircraft in VLOS (Visual Line Of Sight) all the time. Moreover, the remote pilot must keep the UAV at a safe distance from people, and the drone cannot carry any dangerous

goods or drop any material. Therefore, the overall level of risk for UAV operation in the “open” category is low.

Specific (B)

UAV operations in the “specific” category require an operation authorization issued by the competent authority (ENAC in Italy). In this class, the UAVs have no restrictions on the maximum takeoff mass and the maximum altitude. Moreover, the remote pilot can fly in BVLOS (Beyond Visual Line Of Sight). The authorization required varies according to the flight mode (VLOS or BVLOS) and mission specifications. Nevertheless, EASA (European Aviation Safety Agency) and ENAC indirectly are setting up standard scenarios, with which each particular case can be associated. Therefore, the overall level of risk for UAV operation in the “specific” category is medium.

Certified (C)

UAV operations in the “certified” category require the certification of the UAV pursuant to (15), the certification of the operator, and, where applicable, the licensing of the remote pilot. The operations permitted are similar to the previous class, but the UAVs also can carry dangerous goods and even people. Therefore, the overall level of risk for UAV operation in the “certified” category is high.

Italian Regulation

Similarly, the Italian Regulation (10) follows a distinction based on the level of risk of the operation. A primary division hinges on the maximum takeoff mass.

UAVs with a takeoff mass below 25 kg

A primary class is represented by UAVs with a maximum takeoff mass below 25 kg. Moreover, all the drones with a takeoff mass above 250 g must be registered in the D-Flight portal (17) and have a specific QR code stamped on the aircraft. The remote pilots must obtain an attestation of competence in case of professional use, regardless of the weight of the drones, and in case of recreational use, for drones with a weight above 250 g.

Subsequently, operations are divided into non-critical and critical.

Non-critical Operations

Non-critical operations consist of VLOS flights avoiding flying over people and congested areas. In particular, UAVs must keep a distance of 150 m to congested areas and 50 m to people who are not under the remote pilot’s direct control.

In order to run non-critical operations, the remote pilot must complete an online course available on the ENAC website.

Critical Operations

Every operation that does not respect, even partially, the requirements of a non-critical operation is a critical operation. ENAC set up standard scenarios, with which each particular case may be associated. In case the operation is in VLOS and falls within an existing scenario, the operator must present a declaration through the D-Flight portal reporting the flight conditions. Conversely, in case the operation cannot be associated with a standard scenario, including operations in EVLOS (Extended Visual Line Of Sight) and BVLOS, the operator must request the authorization for the flight to ENAC.

In addition to the operation in urban areas, a risk assessment based on SORA documentation issued by JARUS is required. Nevertheless, flying over crowded areas is prohibited.

In order to run critical operations, the remote pilot must complete an online course available on the ENAC website and a specific course of formation at an authorized training center. Regarding EVLOS and BVLOS operations, additional subjects are added to the course of formation.

UAVs with a takeoff mass below 2 kg

Operations involving drones with a takeoff mass below 2 kg are not considered critical in any scenario. However, flying over crowded areas is prohibited.

UAVs with a takeoff mass over 25 kg

UAVs with a takeoff mass over 25 kg must be registered into the ENAC system and the habilitation to fly can be granted by a certification of airworthiness or a fly permit, which is released for research and development purposes or for special operations involving non-serial UAVs. Concerning these last two cases, a risk assessment based on SORA documentation issued by JARUS is required.

Airspace

Airspace is strictly regulated in aviation, and UAVs are not an exception to it. It can be divided into a number of areas, such as airports, heliports, ATZ (Aerodrome Traffic Zone), and CTR (Control Zone). Outside these controlled areas, UAV operations are allowed, without any reservation of the airspace, in case of a flight in VLOS or EVLOS below 120 m (400 ft) of altitude AGL (Above Ground Level) of a drone with a takeoff mass below 25 kg.

Conversely, in the proximity of airports or inside the areas explained above, several limitations are applied to the allowed maximum altitude. Those restrictions are all reported and listed in Circolare ENAC ATM-09 (18). An example is shown in Figure 10, in which a civil airport with instrumental procedures is considered.

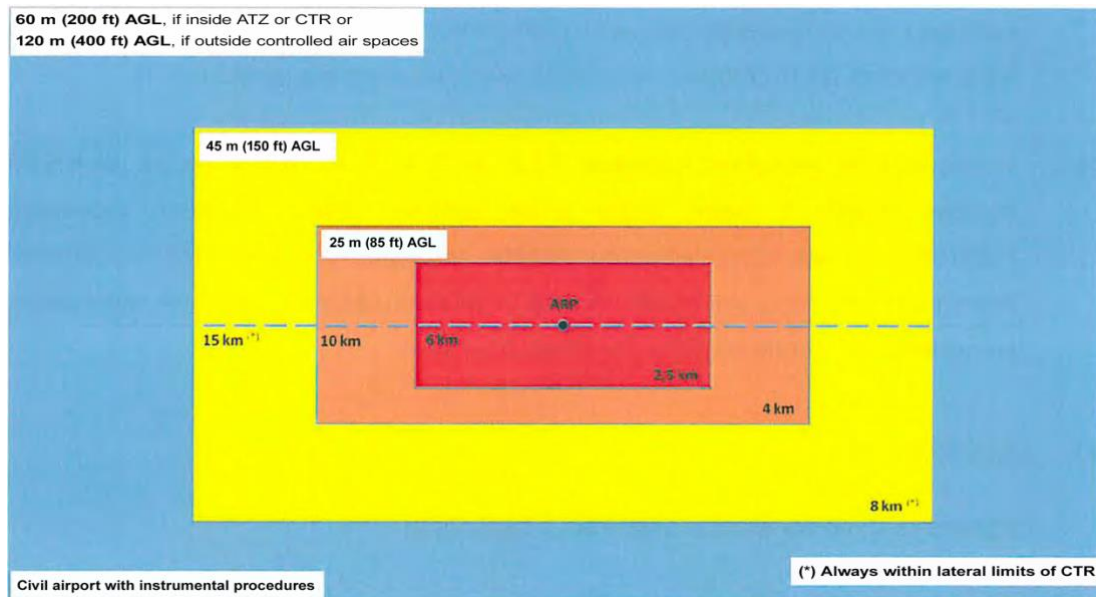


Figure 10 Altitude restrictions when flying close to airports

An explanation of the figure above is provided in the following lines.

- **Red Area.** UAV operations are not allowed within 6 km from the airport, lengthwise either direction of the runway, and 2,5 km sideways.
- **Orange Area.** UAV operations are allowed up to 25 m (85 ft) of altitude AGL within 6 km and 10 km, longitudinally either direction of the runway, and from 2,5 km to 4 km sideways.
- **Yellow Area.** UAV operations are allowed up to 45 m (150 ft) of altitude AGL within 10 km and 15 km, lengthwise either direction of the runway, and from 2,5 km to 4 km sideways.
- **Blue Area.** UAV operations are allowed up to 60 m (200 ft), inside ATZ or CTR, or 120 m (400 ft), outside controlled air spaces, of altitude AGL beyond 15 km longitudinally either direction of the runway, and 8 km sideways.

If the operation requires flying outside those regulated areas, authorization from ENAC to fly in reserved airspaces is needed. Moreover, BVLOS operations could ask for the utilization of segregated airspace, which is for the exclusive use of specific operators for a limited amount of time.

In Figure 11, a picture of the regulated air space in the surroundings of Torino is shown.

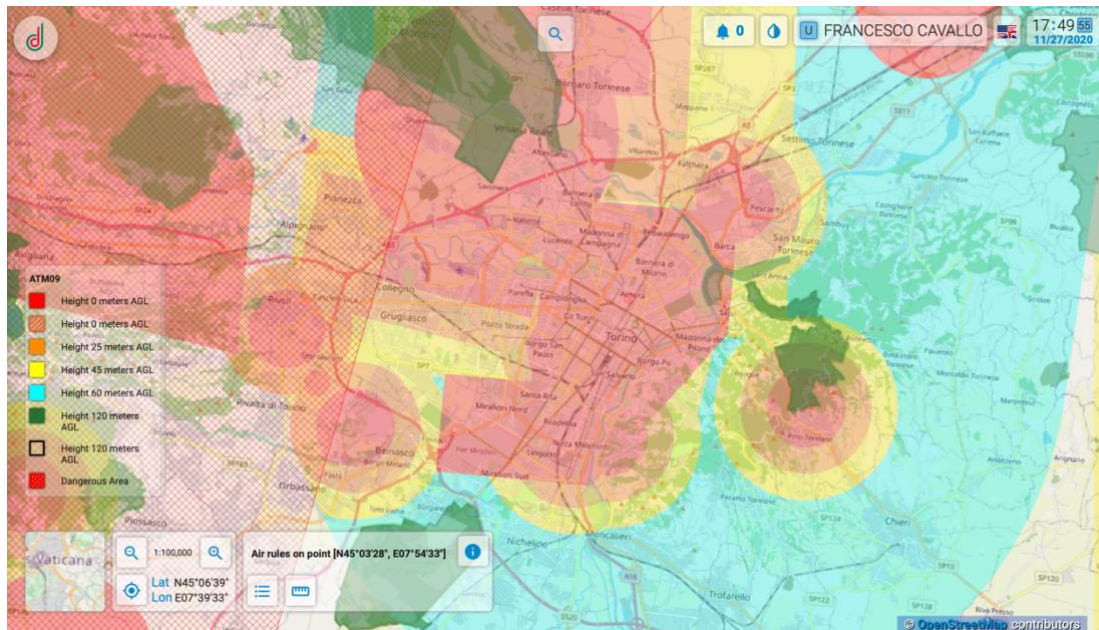


Figure 11 Map of the maximum allowed altitude in Torino area (17)

Effects on the project

As visible in Figure 11, the city of Torino restricts the flight of UAVs in the urban area. Moreover, since the two hospitals selected are apart from each other, the operation must be conducted in BVLOS. Therefore, authorization from ENAC is required.

Since asking for an authorization takes time and must be done for every operation, a trade-off could be achieved in agreement with the regulator authority. Indeed, it would be better to find a different solution together with ENAC, also considering the simulations done in the following chapters. The best option could be a segregated airspace, such as a “corridor” that links the two hospitals. This solution requires more paperwork to start the operations but could be more effective for future developments.

Simulation

In the previous pages, several UAVs were selected to be the best choice for the identified missions and an overview of the regulatory framework has been provided. In this chapter, that information will be utilized for the simulation part of this master's thesis. This section is divided into two areas: the settings to define the environment of the simulation and the explanation of the algorithm utilized.

Settings

As written at the beginning of this master's thesis, two major hospitals, one for each Local Health Unit, have been selected for the simulation. With the help of the doctors Corrado Calvo, Paola Crosasso, and Daniela Cestino, an on-site investigation for each hospital was conducted to find a suitable place for the takeoff and landing of the UAVs. In the following paragraphs, pictures of the site visits are provided. Moreover, a section is dedicated to the UAVs' features considered to run the simulation.

Starting Point

The selected starting point is *Ospedale Molinette* from *Città della Salute e della Scienza di Torino*, situated in the southern part of the city of Torino. This is the largest hospital in the city and the fourth largest in Italy. In Figure 12, it is possible to see a satellite view of it.



Figure 12 Satellite view of Ospedale Molinette

Simulation

It is located in a high populated area without any parks in the surroundings. These aspects represent a difficulty in finding the right place for the takeoff and landing of the drone. Indeed, an isolated area, in which in the undesired case of a fall the risk of damage is minimum, is preferred. Unfortunately, no such areas could be found nearby. Moreover, due to the size of this hospital, a starting point outside it leads to larger times to reach the designated area and, consequentially, larger times to deliver the medicine or biological sample.

Therefore, the search for a suitable place has been conducted inside the structure. Together with the doctor Daniela Cestino, a pharmacist of this hospital, a large, mostly unused terrace has been selected as the starting point of the simulation and UAVs flight. Moreover, the site found is easily accessible from the pharmacy in a short time. In Figure 13 and Figure 14, a satellite and an in-site view of the location is provided. Referring to Figure 12, this area is located in the southern part of the structure.

The characteristics of the designated starting point are:

- **GPS coordinates:** $45^{\circ}02'19.1''$ N $7^{\circ}40'26.4''$ E;
- **Total area:** $19 \times 21 \text{ m}^2 = 399 \text{ m}^2$;
- **Free area:** $12 \times 21 \text{ m}^2 = 252 \text{ m}^2$;
- **Time to get to the pharmacy:** 1 min ;
- **Time to get to the emergency room:** 5 min .

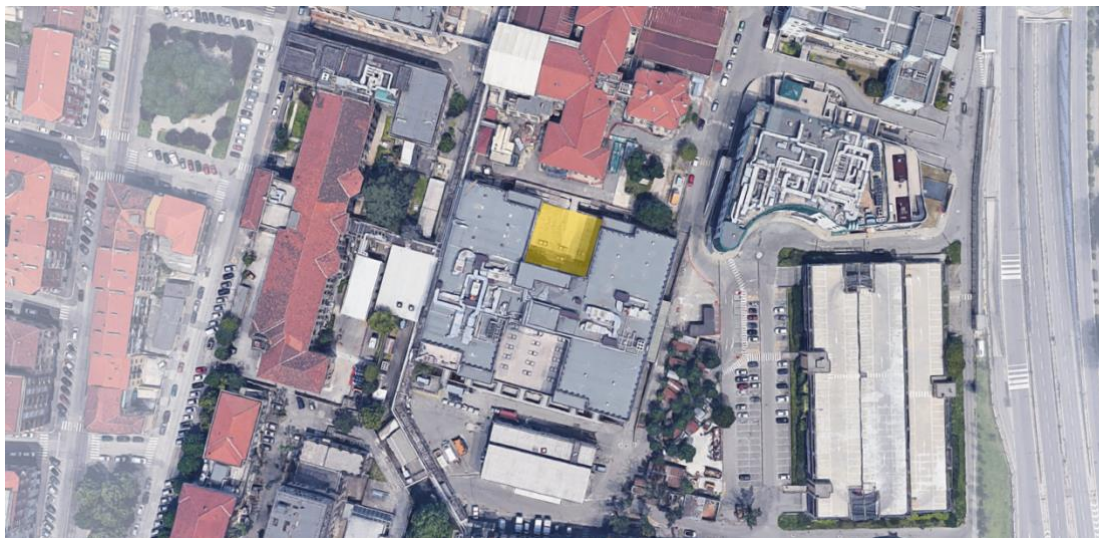


Figure 13 Satellite view of the starting point (yellow area)



Figure 14 In-site view of the starting point

Ending Point

The selected ending point is *Ospedale San Giovanni Bosco* from *ASL Città di Torino*, located in the northern part of the city. This is the largest hospital in the North of the city. In Figure 15, a satellite image of it and its surroundings is shown.



Figure 15 Satellite view of Ospedale San Giovanni Bosco

This hospital is situated also in a high populated area, but this part of the city hosts more parks and low-risk regions. Together with the doctors Corrado Calvo and Paola Crosasso, pharmacists of this hospital, a large unused garden inside the structure has been selected as the ending point of the simulation and UAVs flight. Furthermore, thanks to the size of this hospital, which is much

Simulation

smaller than *Ospedale Molinette*, the selected area could be respectively far from the pharmacy. However, in absolute distances, they are still close enough.

A satellite and an in-site view of this area are shown in Figure 16 and Figure 17. It is clearly visible that other parks are present in the hospital, but the selected one is the only one with an adequate flat area.

The characteristics of the designated ending point are:

- **GPS coordinates:** 45°05'47.3" N 7°42'07.5"E;
- **Total area:** 56x38 m² = 2128 m²;
- **Free area:** 26x26 m² = 676 m²;
- **Time to get to the pharmacy:** 2 min;
- **Time to get to the emergency room:** 1 min.



Figure 16 Satellite view of the ending point (yellow area)



Figure 17 In-site view of the ending point

UAVs' features

During the selection of the drones, all their features were considered to perform a PCA. Now, for the simulation, only few of them, or a combination of them, were utilized to be one of the inputs of the simulation.

Those parameters are:

- Cruise speed in m/s ;
- Maximum flight time in *minutes*;
- Mass in kg ;
- Radius in m ;
- Frontal Area in m^2 ;
- Glide speed in m/s ;

Particular attention must be put on the first two parameters. They can undoubtedly vary throughout an operation. Indeed, they are correlated, suffice it to say that flying at maximum speed will drain the batteries of the UAV more quickly and, consequentially, will reduce the maximum flight time. An insight into this mechanism could be found in the literature (19), which provides an effective instrument to predict the maximum flight time.

Delving into the details, manufacturers usually establish the maximum flight time by hovering the drone under the most favorable atmospheric conditions, such as calm air and low temperature. In the real world, it is hard to get maximum endurance. Furthermore, in this project, UAVs are thought to fly close to their max speed, because of the minimum delivery time required. Hence, they will likely operate in a high-power consumption condition.

Following Hwang, Cha, and Jung's work (19), in which they showed a higher power consumption at high speed, this simulation safely considers half of the declared endurance as the maximum flight time at max speed. In the next section other assumptions has been made concerning the drones' features previously reported.

Algorithm

With the support of Stefano Primatesta, whose work (20; 21) and support have been a fundamental driver for this section of this master's thesis, this segment aims to address the characteristics of the algorithm utilized for the simulation. Therefore, the explanation is divided into two parts. The first concerns the assumptions made, whilst the second regards the process behind the generation of a risk map and optimal trajectory for each drone. More details will also be provided in the next chapter, in which the result will be discussed.

Assumptions

A number of hypothesis on the features utilized has become necessary. This step is crucial to generate a result as close as possible to reality. Here, how some of the parameters are calculated and those mentioned assumptions are reported.

- **Cruise speed.** It is equal to 70% of the UAV's maximum speed achievable declared by the manufacturer. This hypothesis comprises the fact the drone will fly in non-ideal conditions and the influence of the wind.
- **Maximum flight time.** As explained before, it is equal to half of the declared endurance while flying at the cruise speed explained above.
- **Mass.** It comprises the mass of the drone and the payload.
- **Radius.** By looking at a UAV from the top, it corresponds to the radius of the minimum circle that includes the drone. In practice, it is calculated by taking the width or length and dividing it by two.

Simulation

- **Frontal Area.** It is the area of the drone looking at it from a frontal view. It is calculated by multiplying the width and height of the UAV. It is important to estimate the impact area in case of an accident.
- **Glide speed.** It is calculated differently for fixed-wing or multirotor drones. In fact, for the first category, the glide speed is equal to 80% of the declared max speed and it respects the characteristics of an uncontrolled glide. Concerning multirotor UAVs, it is equal to 50% of their declared max speed for a 45° angle glide.
- **Wind.** The city of Torino has an average wind velocity of around 7 km/h (≈ 2 m/s) throughout the year (14). Moreover, the wind has no predominant direction considering the whole year. During the spring and summer months, the wind usually comes from the East. In fall, the predominant direction is North, while in winter, the wind blows primarily from West and North (22). Therefore, considering the low average wind speed and the fact it has no predominant direction, the assumption on the cruise speed being 70% of the maximum speed already covers the wind influence.

Risk Map Layers

The simulation involves the generation of a risk map, which is a geographic map divided into squared cells, for each drone considered. It is useful considering this map as a matrix R , in which each element $R(x, y)$ assesses the risk of the UAV flying over the position (x, y) .

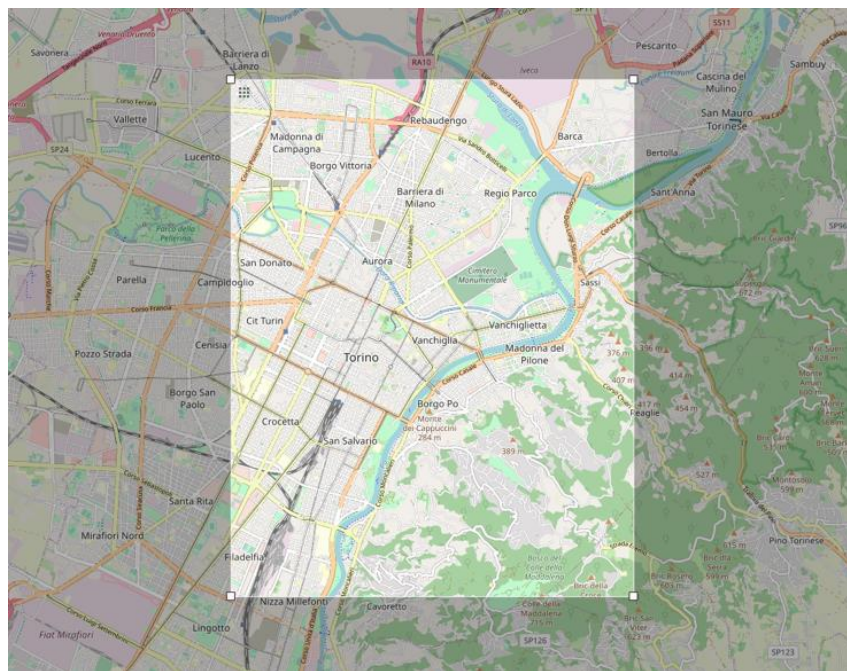


Figure 18 Simulation environment

The definition of risk recalls a typical meter of the aviation world, which is the probability of causing a casualty expressed in hours of flight. Hence, the unit assigned to it is $1/h$. The algorithm utilizes OpenStreetMap (23), an open-source geographic database, to create the basic environment in which the risk is calculated and the path planner operates. In this section, the major features of a risk map are explained.

Referring to Primatesta's work (20; 21), the risk map is a two-dimensional map in which environmental layers and specific UAVs' features, discussed earlier in this chapter, are combined. The result consists of assigning a degree of risk for each cell of the map. The environmental layers refer to the population density, obstacles, sheltering factor, and no-fly zones.

Population density layer

The population density layer refers to the people distribution in the area of interest of the risk map. It covers a critical role in the risk assessment because it is directly linked to the probability of an individual getting involved in a crash of the UAV. Especially in a highly-populated area, such as the city of Torino, which has an average value of $6939 \text{ people}/\text{km}^2$ (24), this layer represents a key factor in the risk map generation process.

The population density layer is a 2D map with the same dimension as the risk map, in which each cell hosts the value of the population density at that specific location. Respecting the same notation as before, it can be defined as a matrix D , in which each element $D(x, y)$ corresponds to a cell of the grid.

Obstacles layer

The obstacles layer concerns the height of obstacles in the risk map. It is created by using OpenStreetMap's database of Torino. Thanks to it, a three-dimensional model of the city can be obtained, and the obstacles layer is produced subsequently. As the risk map, it is a 2D location-based map, in which each cell corresponds to the value of the maximum height of buildings or objects at that specific location. Similarly to the population density layer, it can be defined as a matrix O , in which each element $O(x, y)$ corresponds to a cell of the grid.

The obstacles layer does not take part in the risk assessment. In fact, it has a different role in the risk map generation. For those cells with a maximum height larger than the flight altitude, the obstacles layer defines them as non-flyable zones. On the other hand, for those cells with a maximum height below the flight altitude, the obstacles layer is used to determine the sheltering factor layer by examining all objects and buildings.

Sheltering factor layer

The sheltering factor layer represents the shelter provided by any object to protect the population in case of the crash of the UAV. In particular, it quantifies the level of protection by giving a number from 0 to 10 to diverse areas, according to (25), as reported in Table 4. This layer is crucial for the generation of a realistic risk map since it is responsible for lowering the risk in certain areas. Indeed, the presence of a sheltering element in the crash area allows to reduce the kinetic energy at impact, and, consequently, the probability of a casualty.

Following the notation utilized, the sheltering factor layer can be defined as a matrix S , in which each element $S(x, y)$ corresponds to a cell of the grid. Hence, the corresponding elements of the matrix have one of the values reported in the table below.

Typical Area	Sheltering Factor
No obstacles	0
Sparse trees	2,5
Trees and low buildings	5
High buildings	7,5
Industrial area	10

Table 4 Sheltering Factor

No-fly zone layer

The no-fly zone layer defines the areas in the risk map in which the UAV could not fly. An example is given in Figure 11, in which flying is prohibited in red areas. Regulatory authorities, such as ENAC, could also establish no-fly zones over specific areas, such as military bases and airports. Moreover, some nature-sensitive areas are in this category in order to not disturb the local wildlife. Furthermore, flying in crowded open spaces, such as squares in the city center, is usually forbidden.

This layer also relies on the obstacles layer explained before. Indeed, the UAV cannot fly in a particular area if the maximum height of the buildings or generic objects is larger than the flight altitude. Hence, those cells are identified as no-fly zones.

Respecting the same notation as before, it can be defined as a matrix F , in which each element $F(x, y)$ corresponds to a cell of the grid. Moreover, $F(x, y)$ could be considered as binary, thus

$$F(x, y) = \begin{cases} -1 & \text{flight not allowed} \\ 0 & \text{flight allowed} \end{cases}$$

Once an operation area has been defined, the result of the application of these layers is the same for every drone, since none of its features has been considered so far.

Hazardous Area

The first particularization of the risk map comes with the hazardous area, which is the area occupied by the uncontrolled descent of the drone. Indeed, the UAV will pass through several cells before reaching the ground. Visually, it is useful to think of the hazardous areas as a circle around the UAV, in which it could fall due to a failure. Moreover, different drones and kinds of failure produce different hazardous areas. As written above, the two uncontrolled descents considered are the uncontrolled glide and the ballistic descent.

Uncontrolled glide

The first type of uncontrolled descent of a UAV is the uncontrolled glide. Furthermore, a distinction between fixed-wing and rotary UAVs is required since they show different behavior. In the first case, the drone starts its glide descent with a certain glide ratio, which is the ratio between the horizontal traveled distance and vertical one. As reported in the assumptions, the glide speed is equal to 80% of the maximum speed.

Regarding rotary UAVs, they cannot perform a proper so-called glide. In fact, they do not have any surface that can generate lift. Therefore, the reasonable assumption made has been a descent with a 45° glide angle at 50% of the maximum speed.

Hence, knowing the altitude, it is possible to calculate the distance covered by each kind of UAV during an uncontrolled glide.

$$distance(h) = \gamma \cdot h$$

where γ is the glide ratio and h is the flight altitude.

Ballistic descent

A ballistic descent happens when a UAV cannot generate lift. Therefore, no distinction between the kinds of drones is required. Indeed, the motion depends on gravity and drag only. The classical model could be used to derive its dynamic.

$$m\dot{\mathbf{v}} = m\mathbf{g} - c|\mathbf{v}|\mathbf{v}$$

Where m is the mass of the UAV, c is a constant relative to the drag, g is the gravitational acceleration, and \mathbf{v} is the velocity vector of the drone. Knowing all those UAV's characteristics and its altitude, it is possible to solve the second-order equation written above and find the distance covered by it while it is crashing into the ground.

Risk Assessment

In the lines above, an insight on the concept of risk has been already provided. Thus, it can be defined as the probability of causing at least a casualty per flight hour. The approach used reflects the one commonly utilized in the literature (20; 21; 26). Indeed, a probabilistic methodology has been applied, in which the risk is a combination of three conditional events: the uncontrolled descent of the drone resulting in a crash on the ground, the impact with an individual, and the consequent fatality caused by it. Therefore, the probability of a casualty ($P_{casualty}$) can be defined as

$$P_{casualty} = P_{event} \cdot P_{impact}(x, y) \cdot P_{fatality}(x, y)$$

P_{event} , or failure rate, is the probability of an uncontrolled descent of the drone resulting in a crash on the ground. P_{impact} is the probability of hitting an individual during a failure and a consequent crash on the ground. It is a function of population density and the area exposed to the crash. $P_{fatality}$ represents the probability of the individual to suffer fatal injuries caused by the crash. It depends on the kinetic energy of the UAV at the time of the impact and the sheltering factor.

At this point, it is possible to quantify the risk for each element $R(x, y)$ of the grid by including the particular features of each drone. The result is a specific risk map for each UAV. Indeed, P_{event} , P_{impact} , and $P_{fatality}$ are distinctive for each drone because of the kind of drone, the area exposed to crash, a function of its dimensions, and the kinetic energy, a function of its mass and velocity.

Failure rate

In this project, the failure rate (P_{event}) has been assumed equal to $1/100h$, which means a failure, with a consequent crash on the ground, is expected to happen every 100 hours of flight. Moreover, the UAV can land by an uncontrolled glide or a ballistic descent. For each of them, the failure rate assumed is the same; hence it corresponds to half of the aggregate failure rate ($1/200h$).

Realistically, each drone has associated its own failure rate. However, manufacturers usually do not share this value with customers. Therefore, since the real failure rate is unknown, the assumptions above have been made in order to estimate it. Moreover, providing all the UAVs with the same failure rate value means comparing them only for their performances, such as endurance, cruise speed, and maximum payload weight.

Probability of impact

As defined before, the probability of impact (P_{impact}) is the probability of hitting an individual during a failure and a consequent crash on the ground. The algorithm evaluates it using the equation

$$P_{impact}(x, y) = \rho(x, y) \cdot A_{exp}$$

where $\rho(x, y)$ is the population density, which could be expressed with the population density layer D , and A_{exp} is the area exposed to the crash. This area can be defined as

$$A_{exp}(\theta) = 2(r_p + r_{UAV}) \frac{h_p}{\tan(\theta)} + \pi(r + r_p)^2$$

where r_p and h_p are respectively the radius and height of a person, considering him or her as a cylinder, r_{UAV} is the radius of the UAV and θ in the angle of the impact on the ground. Thus, the only variable is the angle θ since it depends on the type of uncontrolled descent.

Since the UAV could impact on the ground in every point of the hazardous area defined above, a georeferenced two-dimensional probability density function (PDF) is used to describe the ground impact area. Then, the probability of impacting on a person could be written as

$$P_{impact}(x, y) = \sum_{x,y} PDF \cdot D(x, y) \cdot A_{exp}(\theta(x, y)).$$

Probability of fatality

Evaluating the probability of a fatality ($P_{fatality}$) caused by the impact of an uncontrolled UAV is not simple. Indeed, drones could impact in several ways and locations in an individual's body. Also, different people could respond in different ways on the same impact. The algorithm approached the problem by calculating this probability using the kinetic energy at the impact and the sheltering factor. Indeed, buildings and obstacles help to reduce the kinetic energy at the impact. Hence, the probability of a fatality decreases in areas which a higher sheltering factor.

Likewise the calculation of the probability of impact, the algorithm uses a georeferenced two-dimensional probability density function (PDF) to describe the expected value of the kinetic energy at impact and sheltering factor for each location (x, y) . Therefore, the probability of a fatality can be obtained as

$$P_{fatality}(x, y) = \frac{1 - k}{1 - 2k + \sqrt{\frac{\alpha}{\beta}} \left[\frac{\beta}{\Lambda[E_{imp}(x, y)]} \right]^{\frac{3}{\Lambda[S(x, y)]}}}$$

where $k = \min \left(1, \left[\frac{\beta}{\Lambda[E_{imp}(x, y)]} \right]^{\frac{3}{\Lambda[S(x, y)]}} \right)$, $S(x, y)$ is the sheltering factor at that specific location, E_{imp} is the kinetic energy at the impact, α is the impact energy needed to obtain a fatality probability of 50 % when $S(x, y) = 6$, and β is the impact energy needed to cause a fatality when $S(x, y)$ reaches zero. Moreover, the function Λ represents

$$\Lambda[E_{imp}(x, y)] = \sum_{x, y} PDF \cdot E_{imp}(x, y) \quad \text{and} \quad \Lambda[S(x, y)] = \sum_{x, y} PDF \cdot S(x, y).$$

Concerning the sheltering factor, it is extracted by using the sheltering factor layer S . On the other hand, the kinetic energy at the impact is evaluated according to the uncontrolled descent type. The relation used to estimate it recalls the typical kinetic energy equation

$$E_{imp}(x, y) = \frac{1}{2} m \cdot v_{imp}(x, y)^2$$

where m is the UAV's mass and v is its velocity at the impact. Regarding the uncontrolled glide, the velocity at the impact is the glide speed considered. In the ballistic descent case, the velocity at the impact can be obtained through the combination of its horizontal and vertical velocities, which are the solutions of the second-order motion equation.

Layers Combination

Once all layers have been defined, the last step consists of merging them to generate the risk map associated with a certain UAV. In particular, the obstacles layer and the no-fly zone layer are joined to define non-flyable areas, which occurs when $F(x, y) = -1$ or $O(x, y) \geq h$, where h is the flight altitude of the drone. Similarly, risk map elements are defined as

$$R(x, y) = \begin{cases} -1 & \text{if flight not allowed} \\ P_{casualty}(x, y) & \text{if flight allowed} \end{cases}$$

Thus, the probability of a casualty is obtained as the combination of

$$P_{casualty}(x, y) = P_{casualty}^{un.glide}(x, y) + P_{casualty}^{bal}(x, y)$$

where the terms on the right side of the equation represent the probabilities of casualty according to the uncontrolled descent type. Since they are interdependent within them, they can be simply added to each other.

An example of the resulting risk map is reported in Figure 19. It is the product of this whole procedure, and it is capable of showing, in a single picture, all the information collected on the drone and the flight area. Those risk maps are unique for each UAV, and they will be used in computing the optimum risk-aware path. Moreover, they represent a great instrument to evaluate the risk of flying a drone for the population in a certain area.

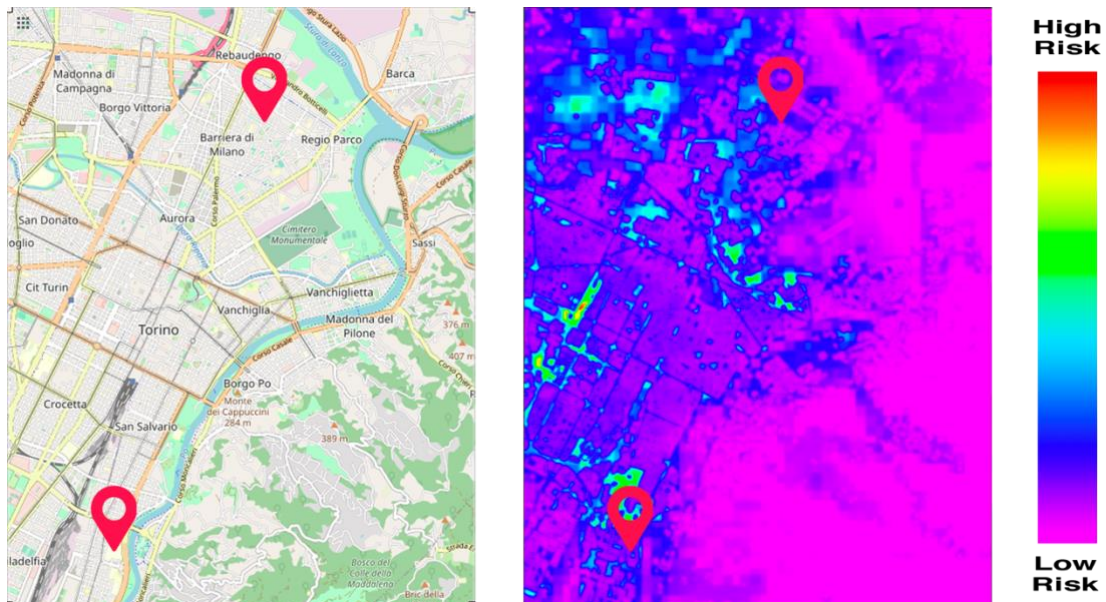


Figure 19 Example of DJI Matrice 200's risk map

Path Planning

Once every drone analyzed has got its associated risk map, it is possible to compute the optimal trajectory from *Ospedale Molinette* to *Ospedale San Giovanni Bosco*. In this case, the optimal trajectory means the path that minimizes the risk (given by the risk map) and the flight time. Indeed, it is critical to remember the application for which this setup is thought: medicine delivery during emergencies.

The optimal path is generated using the Optimal Rapidly-exploring Random Tree (RRT*) algorithm. It is a sample-based method that explores the search space with an incremental tree, in order to minimize the motion cost. Moreover, as explained above, risk values are expressed per hour of flight, and the probability of causing a casualty depends on the individual's exposure to the risk. This dependency is the result of the complex system to evaluate the probability of a failure. In the next chapter, a better comprehension of this aspect will be given. Indeed, the path planner faces situations in which a tradeoff between the absolute risk (provided by the risk map) and the person's exposure to it is required.

Results

After carefully analyzing how the simulation process has been carried out, in this chapter, the result will be presented and discussed. As explained above, the output of the simulation is the risk-aware path, expressed in GPS waypoints, together with several data about it. Also, a 3D simulation of the flight of the two main distinctive UAVs (Matrice 200 V2 and Phantom 4 RTK) is provided.

The simulation took the UAVs selected using the PCA method. However, some of them have similar features; thus, a selection of them has been performed. Two different conditions have been used for the simulation. The first one considers the flight altitude as 50 m, whilst, for the second one, the flight altitude is set at 20 m. The difference between them will be explained in the following pages.

Risk Map and Trajectory (altitude 50 m)

In Table 5, the results of the simulation are presented. The risk-aware path planner returns several features of the trajectory. For instance, the first column regards the risk involved during the mission. As explained before, it is defined as casualties per flight hour. A suitable and highly used value for the maximum acceptable risk is $1 \cdot 10^{-6} h^{-1}$, as reported in the literature (27). Therefore, the computed risk must be lower than that value. None of the drones tested nevertheless respects this limitation, but their average values have at least the same order of magnitude, except the WingatraOne. In fact, it has an average computed risk around $1 \cdot 10^{-5} h^{-1}$, which lists it as the most dangerous for this application. However, the maximum acceptable risk is usually a conservative measure to keep a safety margin. Indeed, other documents (28) establish higher values for the maximum acceptable risk, such as $3 \cdot 10^{-5} h^{-1}$ or $2 \cdot 10^{-4} h^{-1}$, depending on the operation. In this case, all UAVs analyzed are considered safe for the flight. Moreover, this project regards emergency protocols, which usually accept a higher degree of risk. Hence, the safety of the UAVs selected is within the permitted limits.

Differently, the trajectory cost is a dimensionless number that represents a way to evaluate the overall performance of a drone. It also explains the tradeoff required between the path safety and the duration of the operation. Indeed, looking at the dimensions of the terms on the right side of its expression below,

Results

	Avg. risk $[1/h]$	Trajectory cost	Path length $[m]$	Duration of FF² $[s]$
eBee SQ/X	$2,404 \cdot 10^{-6}$	$1,317 \cdot 10^{-3}$	11502	548
Evo II	$1,406 \cdot 10^{-6}$	$1,019 \cdot 10^{-3}$	9127	724
Falcon x8	$7,461 \cdot 10^{-6}$	$6,971 \cdot 10^{-3}$	9811	934
Matrice 200 v2	$7,338 \cdot 10^{-6}$	$4,493 \cdot 10^{-3}$	9429	612
Mavic 2	$2,069 \cdot 10^{-6}$	$1,361 \cdot 10^{-3}$	8287	658
Phantom 4 RTK	$1,732 \cdot 10^{-6}$	$1,023 \cdot 10^{-3}$	8273	591
WingtraOne	$1,496 \cdot 10^{-5}$	$1,155 \cdot 10^{-2}$	8649	772

Table 5 Simulation outcome at 50 m of altitude

the trajectory cost informs about the fatalities throughout the mission. Hence, UAVs with lower trajectory cost are more efficient in that tradeoff, while drones with higher trajectory cost are not.

$$\text{Trajectory Cost} = \frac{\text{Path Length} \cdot \text{Avg. Risk}}{\text{Velocity}}$$

Moreover, the total length of the trajectory is the result of the tradeoff between the risk and the need to complete the operation in the minimum time possible. It will be more visible in the figures below, in which all the trajectories are reported. The algorithm also provides the duration of the forward flight as a result.

Table 6 shows the total duration of the mission. Indeed, using the duration of the forward flight together with the climbing and descent phases, an overall flight time could be estimated. The algorithm operates considering a fixed-altitude flight, which has been set to 50 m. Hence, the time used to get at the operational altitude can be easily found by taking into account the maximum climb speed of the UAVs.

² Forward Flight duration. Takeoff and landing are excluded for now.

$$\text{climbing/descent time} = \frac{50 \text{ m}}{\text{climbing/descent speed}}$$

It is important to highlight that, for both versions of the eBee, the climb rate is zero. The reason behind it lies in the fixed-wing type of aircraft because it needs to move forward to gain altitude. Hence, climbing has been already considered in the forward flight duration.

Similarly, the same process could be done for the time used for the descent phase.

	Duration of FF [s]	Climb speed [m/s]	Descent speed [m/s]	Total Duration [s]
eBee SQ/X	548	0	0	548
Evo II	724	8	4	743
Falcon x8³	934	5	3	961
Matrice 200 v2	612	5	3	639
Mavic 2	658	5	3	684
Phantom 4 RTK	591	6	4	613
Wingatra One	772	6	1	831

Table 6 Total flight duration at 50 m of altitude

In order to find differences among similar UAVs, a common practice is to divide them into categories. Indeed, the main clusters are the fixed-wing, small-size multirotor, and mid-size multirotor UAVs. Indeed, the risk maps associated to the drones of the same class are similar as well as the computed optimum trajectory. Furthermore, concerning the maximum and minimum value of the computed risk of the map, they also present some similarities. Indeed, they are similar within UAVs of the same category. The reason must be pursued in the risk maps, which highly depend on dimensions and weight of the drones.

³ Climb and descent speed values has not been found; hence, they were assumed equal to Matrice 200 V2 ones, due to their similar characteristics.

Fixed-wing

The first cluster concerns the UAV equipped with a fixed-wing. This feature usually provides high endurance because the wing generates lift instead of the propeller. Therefore, most of the energy is consumed for the forward flight. The drones included in this cluster are the eBee SQ, eBee X, and WingtraOne. Among them, the eBee family requires an initial forward velocity to takeoff and an obstacle-free site where to land. On the other hand, the WingtraOne can take off and land vertically, thanks to the combination of its propellers and flaps.

eBee SQ/X

The resulting risk map associated with the eBee SQ and the eBee X is shown in Figure 20. The maximum and minimum risks on the map are $2,437 \cdot 10^{-5} h^{-1}$ and $2,975 \cdot 10^{-7} h^{-1}$, respectively. It is possible to distinguish the hilly area on the right side (fuchsia color), where the population density is lower than the rest of the city. Hence, the risk associated with it is low. Another distinctive area is the Po river, which is associated with a medium level of risk. Indeed, in the dark blue area in the center of Figure 20, it is possible to spot its silhouette.

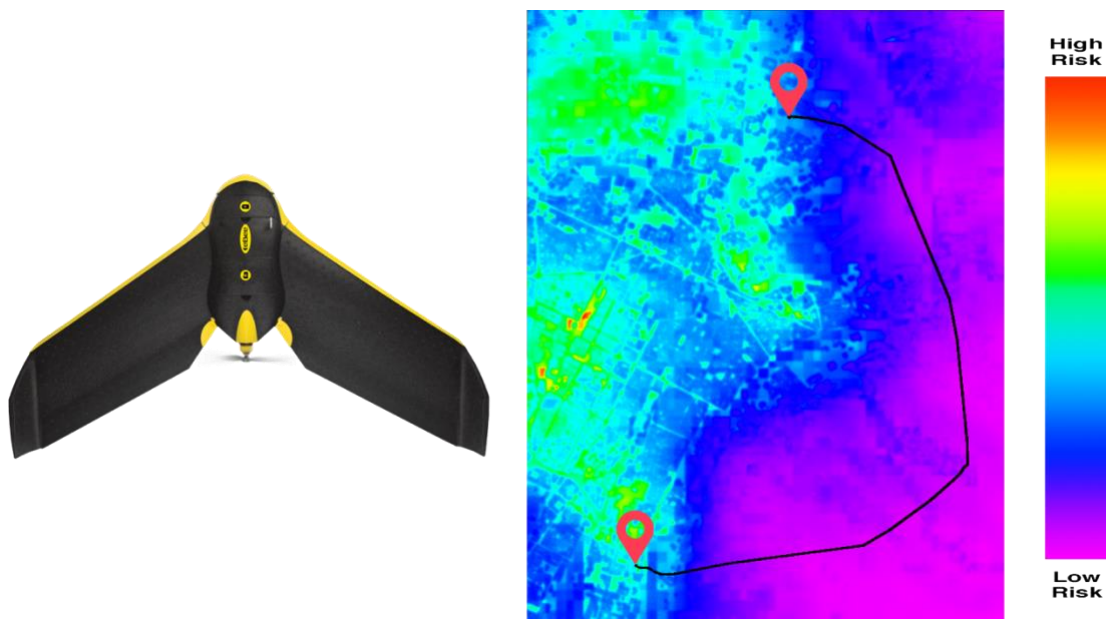


Figure 20 eBee X (on the left) and its risk map and optimum trajectory at 50 m of altitude (on the right)

Concerning the city center, on the left part of the picture (green color), the high level of risk of that area forces the path planner to compute a trajectory to avoid it. Therefore, this UAV will fly over the hills to compensate for the higher risk level of the areas of takeoff and landing.

Another significant aspect is the uniformity of the risk level of the map. Comparing this risk map to the one of the Evo II in Figure 22, it is noticeable

that, for the eBee SQ/X, there are distinct low-risk and high-risk areas, while they are mixed for the Evo II. This characteristic is peculiar to the fixed-wing category. Indeed, the high cruise speed and frontal area of the drones make their hazardous areas and probability of impact larger than other UAVs. Hence, these aspects can be encountered in their risk maps.

Although the eBee SQ/X could link the two hospitals in the least amount of time, even if the longer path length, they cannot be considered as a solution for this project. In fact, this type of aircraft brings the need for a dedicated site for landing, since it has a fixed-wing. On the other side, the takeoff could be done by hand. In an urban area, this aspect represents a problem that hardly can be solved. A UAV, capable of a vertical takeoff and landing, would be preferred.

WingtraOne

The WingtraOne developed by Wingra is a fixed-wing UAV capable of vertical takeoffs and landings. The risk map associated with it is reported in Figure 20. The maximum and minimum risks on the map are $2,496 \cdot 10^{-4} h^{-1}$ and $5,422 \cdot 10^{-7} h^{-1}$, respectively.

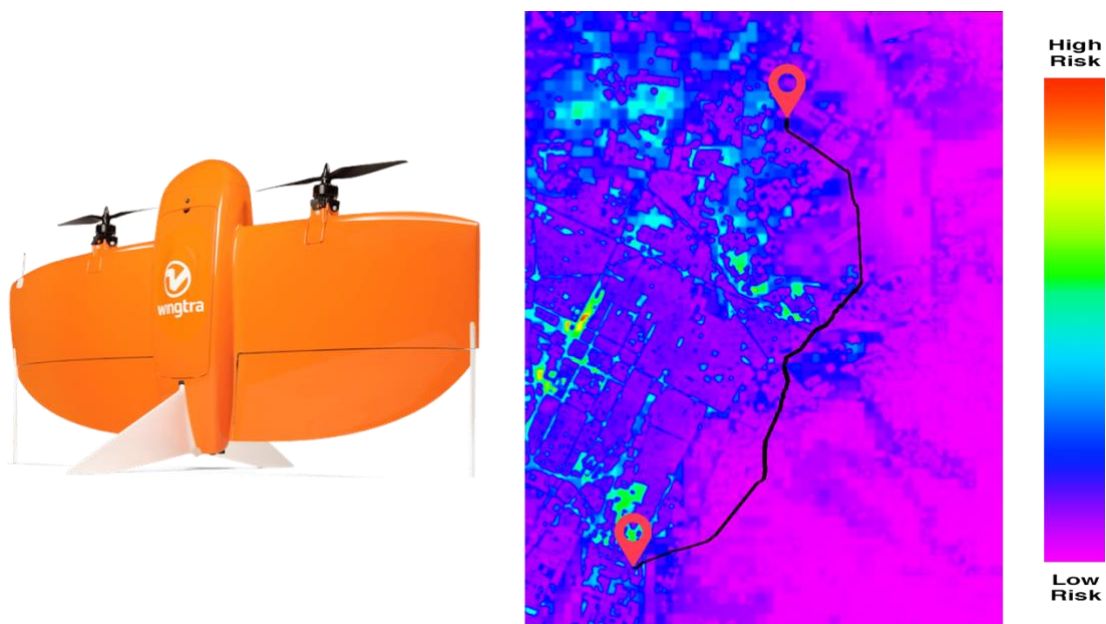


Figure 21 WingtraOne (on the left) and its risk map and optimum trajectory at 50 m of altitude (on the right)

Despite the similarities to the eBee family, its cruise speed is almost a third of the cruise speed of the eBee SQ/X. Therefore, its risk map is comparable to the ones obtained with the multirotor class, since a lower cruise speed implies smaller hazardous areas. However, the average risk of the path is almost twice as the other UAVs analyzed. The reason to explain it relies on the dimension of the WingtraOne. Indeed, having a low cruise speed is not enough to balance the

Results

increased probability of an impact with a person in case of failure due to its large frontal area.

However, its low cruise speed entails a longer duration of the mission, which is a significant deficit for this project.

Small-size Multirotor

The second cluster analyzed regards the small-size multirotor UAVs. The reason lies in the regulatory framework. As written in the dedicated chapter, lighter drones have more freedom to fly than heavier ones. Therefore, it would be easier to get the clearance from ENAC for flying over an urban area. However, these UAVs are able to carry only a light payload; hence, they could be used only for the transportation of a few doses of antidotes.

In comparison with the fixed-wing cluster, the computed risk-aware trajectory directs the small drones towards areas with a higher population density. Thus, they have shorter path lengths since they can fly over the city center.

The drones included in this cluster are the Evo II, the Mavic 2, and the Phantom 4 RTK. They have similarities in their risk maps and trajectory. For instance, the first part of the journey is almost the same for all three. They avoid the highly populated area in the North of the starting point, *Ospedale Molinette*, by going to the hills at the bottom right of the map. Then, their paths became different when a solution to deal with crossing the city center must be found.

Evo II

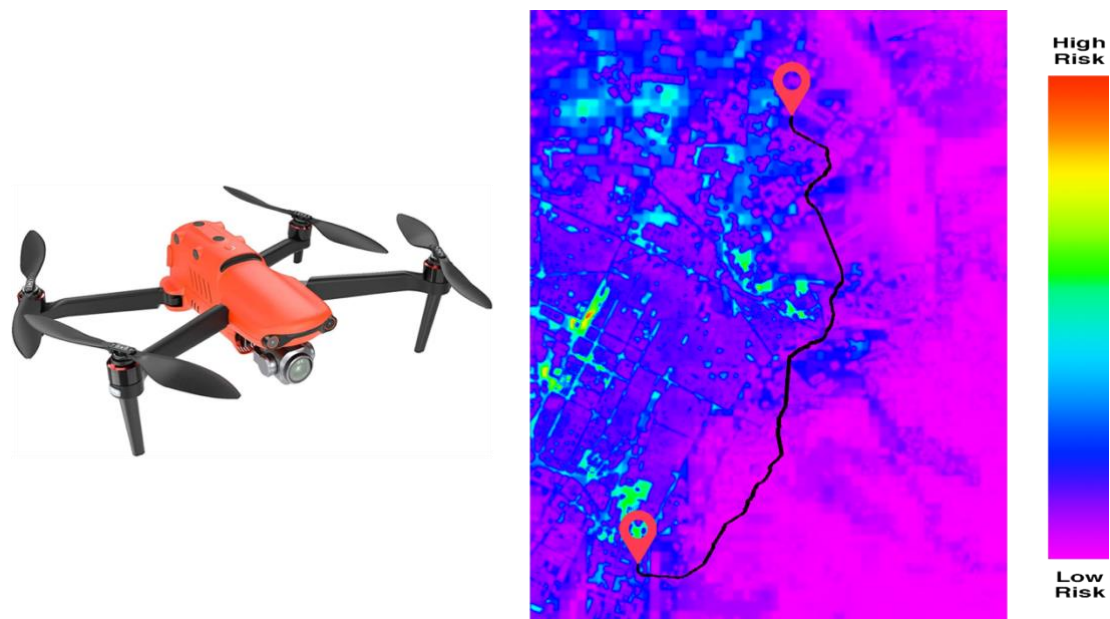


Figure 22 Evo II (on the left) and its risk map and optimum trajectory at 50 m of altitude (on the right)

The first UAV of the small-size multirotor class is the Evo II from Autel Drones, whose risk map and trajectory are shown in Figure 22. The maximum and minimum risks on the map are $2,698 \cdot 10^{-5} h^{-1}$ and $2,646 \cdot 10^{-8} h^{-1}$, respectively.

It takes longer than the other two drones of this class to get to the ending point. The reason could be found in the center of its risk map. Indeed, unlike the Mavic 2 or the Phantom 4 RTK, it avoids the high-risk areas in the center of Figure 22, which are represented by three green spots in the middle. This deviation is the main difference between them.

Mavic 2

The second UAV of the small-size multirotor family is a well-known drone used for several scopes, the Mavic 2 from DJI. Its risk map and optimal trajectory are displayed in Figure 23. It is similar to other same-class drones; however, it is not the quickest one to get to the destination. The maximum and minimum risks on the map are $3,235 \cdot 10^{-5} h^{-1}$ and $2,913 \cdot 10^{-8} h^{-1}$, respectively.

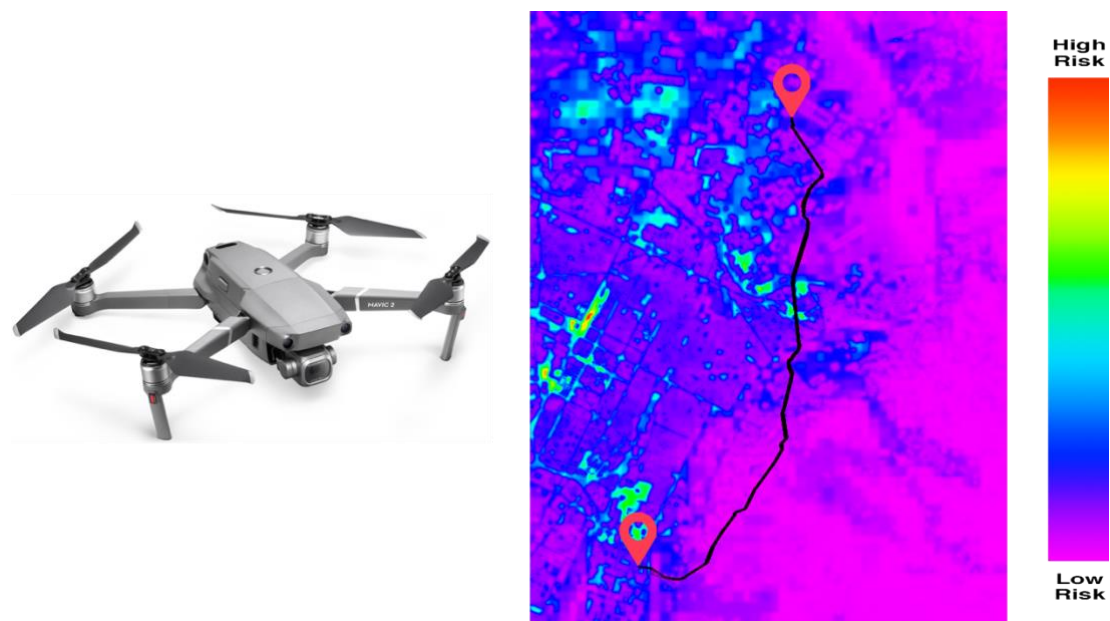


Figure 23 Mavic 2 (on the left) and its risk map and optimum trajectory at 50 m of altitude (on the right)

The main difference compared to the previous drones is located in the center of the risk map. Indeed, the risk-aware path planner declared that flying closely over the central high-risk area, represented by three green spots in the middle, is safe. This behavior could be explained by referring to the calculation of the risk and the path. Indeed, the risk-aware path planner aims to find the optimum trajectory in which the average computed risk is minimum. Therefore, crossing or flying nearby a high-risk area for a small period of time is sometimes beneficial for the overall result.

Its trajectory is almost the same as the Phantom 4's one, but it differs in two regions. The first one is almost at the half of the path, in which the Mavic 2 crosses the river Po earlier. The second one is at the end of the journey. In this case, the Mavic 2 goes around a certain area while the Phantom 4 opts for a straighter trajectory.

Phantom 4 RTK

The last small-size multirotor UAV analyzed is the Phantom 4 RTK from DJI. It has the same notoriety as the Mavic 2, and, as already explained above, almost the same characteristics. Its risk map and optimal trajectory are reported in Figure 24. The maximum and minimum risks on the map are $2,808 \cdot 10^{-5} h^{-1}$ and $2,223 \cdot 10^{-8} h^{-1}$, respectively.

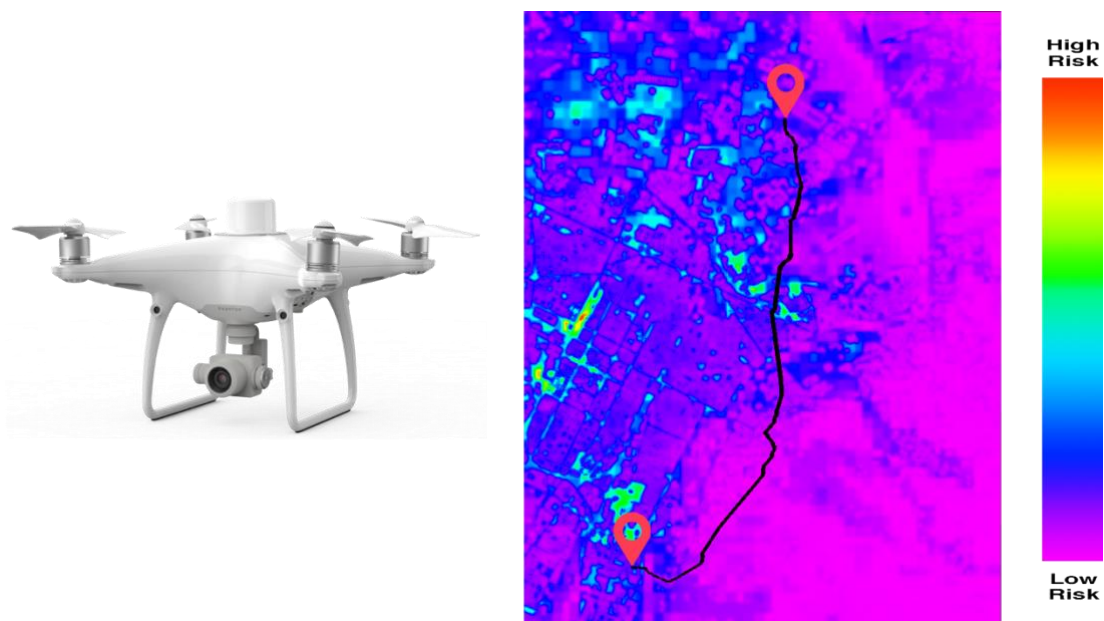


Figure 24 Phantom 4 RTK (on the left) and its risk map and optimum trajectory at 50 m of altitude (on the right)

The risk-aware path planner also computes that it is safer for it to fly closely over the central high-risk area, represented by three green spots in the middle as well as the Mavic 2. The main differences between these two similar UAVs are the overall path length and duration and physical appearance. While the first two depend on its features and how the risk assessment is performed, the last one is crucial to choose as the best option for the small-size multirotor family. Indeed, the Phantom 4 RTK has got a shape that better allows the storage of a small payload underneath the fuselage. Therefore, being the quickest one to be able to get to the ending point and most appropriate to carry a payload make it the best among the others in this cluster.

For the reasons above, the Phantom 4 RTK has got displayed in a 3D environment the optimum trajectory shown in Figure 24. This more realistic visualization helps the operators to feel that they are in a real flight.

Mid-size Multirotor

The last cluster analyzed is the mid-size multirotor family. The regulatory authorities apply more restrictions for UAVs of this class, due to their weight. On the other hand, they can carry larger payloads, compared to the previous classes, while keeping high cruise velocities. Therefore, these drones could also be used for transporting biological samples or blood products as well as high priority antidotes.

In comparison with the small-size multirotor class, they show an overall higher-risk, due to their larger weights and dimensions. Indeed, they avoid the central area of the city, passing through the eastern side. Hence, their path lengths are longer than smaller UAVs.

The drones included in this cluster are the Falcon x8 and the Matrice 200 V2. They have similarities in their risk maps and trajectory. However, the second one shows straighter lines in its trajectory, allowing it to have the shortest path between the two.

Falcon x8

The first mid-size multirotor UAV analyzed is the Falcon x8 from Airborne Drones.

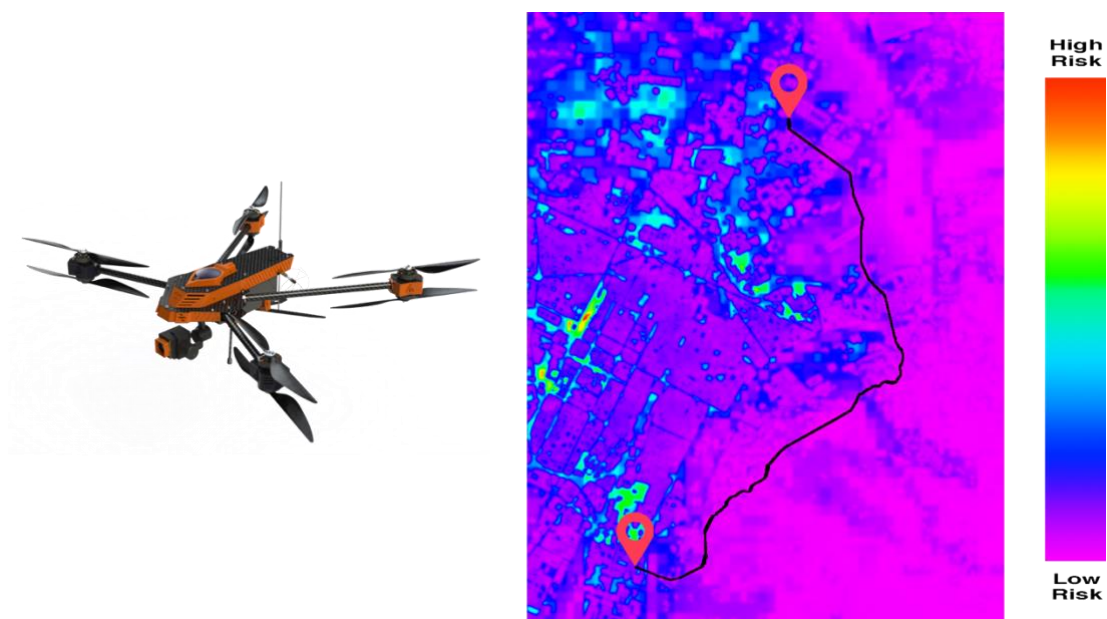


Figure 25 Falcon x8 (on the left) and its risk map and optimum trajectory at 50 m of altitude (on the right)

It is the only drone having contra-rotating propellers. Nevertheless, this feature does not affect this analysis, whose result is shown in Figure 25. It is also the slowest drone among all categories. The reason lies in the application for which it was designed, mapping and surveillance. Hence, he does not have a high cruise speed and, due to its weight and dimensions, the risk-aware path planner has listed it as the second-longest trajectory among all. However, for these reasons, the Falcon x8 is not the optimal option for this family.

In Figure 25, the results of the simulation are shown. The risk map is almost the same as the Matrice 200's one, but its path is more twisted than the other. The maximum and minimum risks on the map are $1,972 \cdot 10^{-4} h^{-1}$ and $1,689 \cdot 10^{-7} h^{-1}$, respectively.

Matrice 200 V2

The second mid-size multirotor UAV analyzed is the Matrice 200 V2 from DJI. As well as the other drones produced by the same company, it is a well-known drone used for several scopes. Its risk map and computed optimum path are displayed in Figure 26. The maximum and minimum risks on the map are $1,698 \cdot 10^{-4} h^{-1}$ and $1,786 \cdot 10^{-7} h^{-1}$, respectively.

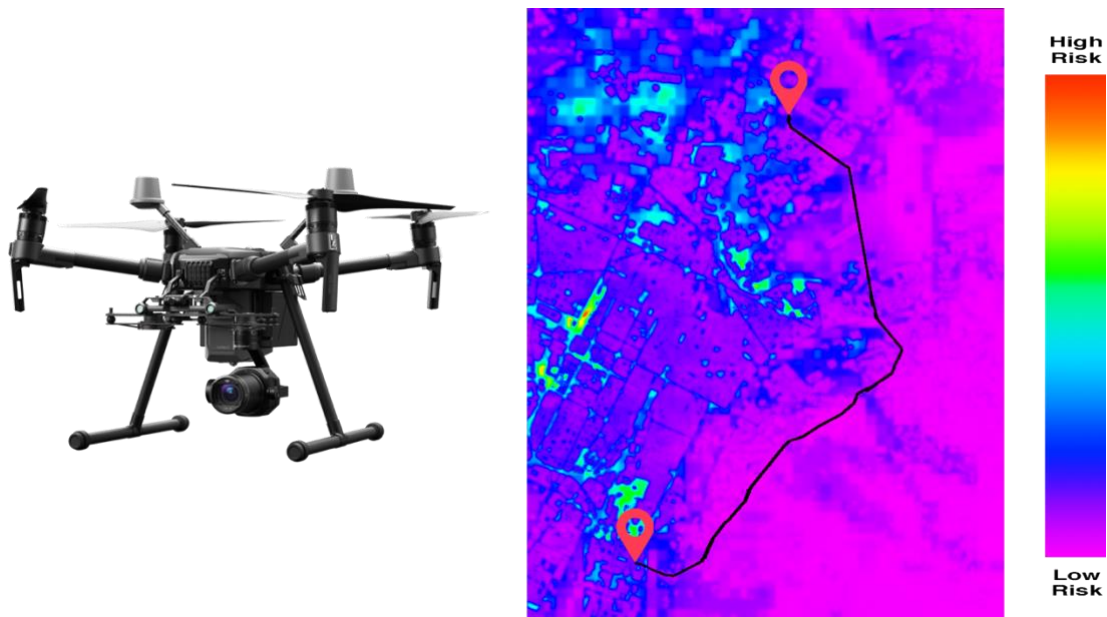


Figure 26 Matrice 200 V2 (on the left) and its risk map and optimum trajectory at 50 m of altitude (on the right)

It is the fastest one among all multirotor UAVs. Moreover, it has a similar but smoother path compared to the other drone in the same category. Indeed, as the Falcon x8, it avoids the highly populated area located in the North of the starting point. The risk-aware path planner prefers directing it over the hills, the bottom right side of Figure 26. It changes direction to cross the river Po and to proceed towards the ending point.

Its high cruise speed allows it to be also the quickest drone, apart from the eBee SQ/X, to reach the destination. This aspect makes him the best choice for this class. Moreover, later in this chapter, a 3D visualization of its journey is provided.

Risk Map and Trajectory (altitude 20 m)

Furthermore, in order to find shorter paths, another simulation at 20 m of altitude has been performed. This analysis aims to lower the risk by reducing the hazardous area. Indeed, flying at a low altitude decreases that area; thus, the path planner could compute a trajectory that exploits the narrow low-risk area in the city center. On the other hand, the obstacles layer becomes predominant at low altitude. In fact, the presence of buildings or objects interferes with the generation of the optimum path. By listing more cells of the risk map as no-fly zones, the drone must avoid those with the risk of increase the total length of the trajectory. For this simulation, only the best options among the drones analyzed above have been considered; hence, the Phantom 4 RTK and the Matrice 200 V2. The results are reported in Table 7 and Table 8.

	Avg risk $[1/h]$	Trajectory cost	Path length $[m]$	Duration of FF $[s]$
Phantom 4 RTK	$1,879 \cdot 10^{-6}$	$1,210 \cdot 10^{-3}$	9021	644
Matrice 200 V2	$7,870 \cdot 10^{-6}$	$4,365 \cdot 10^{-3}$	8542	555

Table 7 Simulation outcome at 20 m of altitude

Comparing these results with the ones at 50 m of altitude in Table 5, the computed risk for the Phantom 4 is almost the same as the previous scenario. Contrarily, the trajectory cost slightly increases due to the rise of the computed path length. Therefore, the time spent in the forward flight also increases.

Concerning the Matrice 200 V2, it also shows a similar computed risk with a soft increase in the average risk of the path and a slight drop of the minimum risk. The trajectory length decreases by 9,4 %, but the trajectory cost remains almost the same, balancing off the diminished path length and the increased average risk.

In comparison to the result calculated at 50 m of altitude in Table 6, the total duration varies in different ways for the drones considered. The Phantom 4, for instance, has an increased overall flight time of 10,5 %, while the Matrice 200 V2 turns itself into the quickest drone to link the two hospitals by lowering the

Results

total duration by 7,7 %. A more detailed explanation is provided in the lines below.

	Duration of FF [s]	Climb speed [m/s]	Descent speed [m/s]	Total Duration [s]
Phantom 4 RTK	644	6	4	653
Matrice 200 V2	555	5	3	565

Table 8 Total flight duration at 20 m of altitude

Phantom 4 RTK

The Phantom 4 RTK, already explained in the previous section, reveals different risk maps and, consequentially, different computed optimal paths at the altitudes considered. The maximum and minimum risks on the map are $2,795 \cdot 10^{-5} h^{-1}$ and $1,826 \cdot 10^{-8} h^{-1}$, respectively. In Figure 27, those differences are shown. Indeed, the risk map on the left (at 20 m of altitude) is more detailed due to the smaller hazardous area involved. Therefore, the risk is less distributed across the map. On the other hand, an altitude of 20 meters means that all buildings with more than six floors are considered as a no-fly zone. Indeed, the obstacles layer gains more importance.

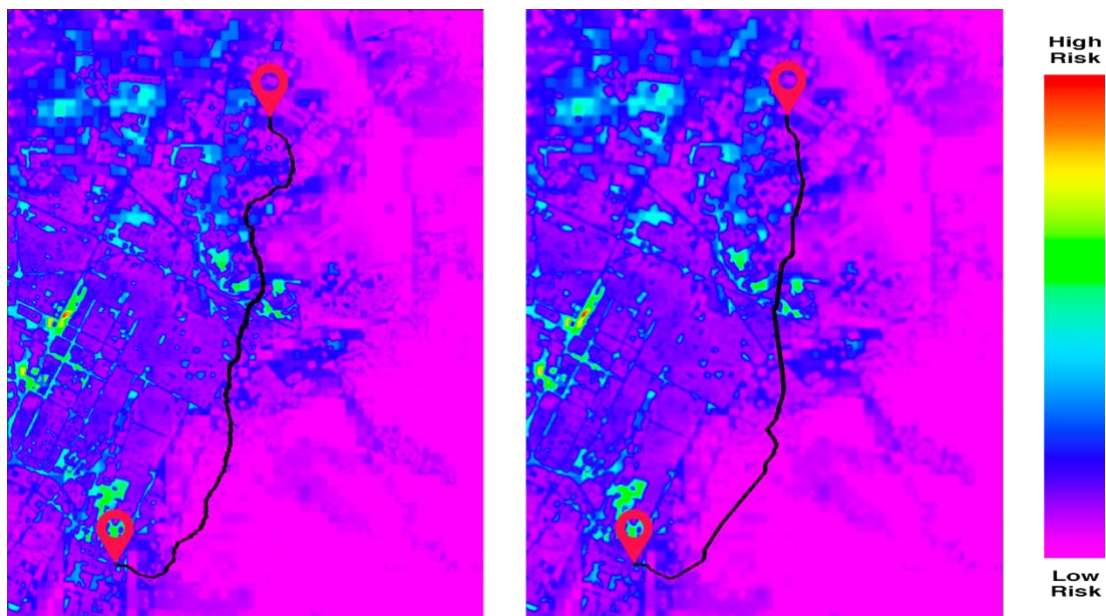


Figure 27 Phantom 4 RTK risk map and optimum trajectory at 20 m of altitude (left) and at 50 m of altitude (right)

Although the risk-aware path planner guides the drone through the city center, the result is a more twisted trajectory in order to avoid no-fly zones, which

means the overall path length increases. Hence, lowering the altitude to 20 m does not pay off. In fact, the ability to better discern low and high-risk areas is not balanced by the presence of more obstacles than before.

Matrice 200 V2

The Matrice 200 V2 shows similar behavior in respect to the Phantom 4 regarding the more detailed risk map. The comparison of the two risk maps at different altitudes is reported in Figure 28. The maximum and minimum risks on the map are $1,754 \cdot 10^{-4} h^{-1}$ and $9,026 \cdot 10^{-8} h^{-1}$, respectively. By better discerning low and high-risk areas, the UAV can cross the river Po earlier, as it is possible to see in the center of the image. Indeed, the risk-aware path planner makes the drone to fly over more central areas.

Contrarily to the case of the Phantom 4, this UAV shows a smoother trajectory. This aspect could be explained as the higher average computed risk of the Matrice 200. Besides a more detailed risk map, the mass and dimensions of this drone are the factors that increase the risk of impact on a person and the consequent fatality. Therefore, it tends nevertheless to avoid high-populated areas, which are usually the ones with taller buildings. As a consequence, the computed optimal trajectory is shorter at an altitude of 20 m. Hence, reducing the altitude brings more benefits than drawbacks.

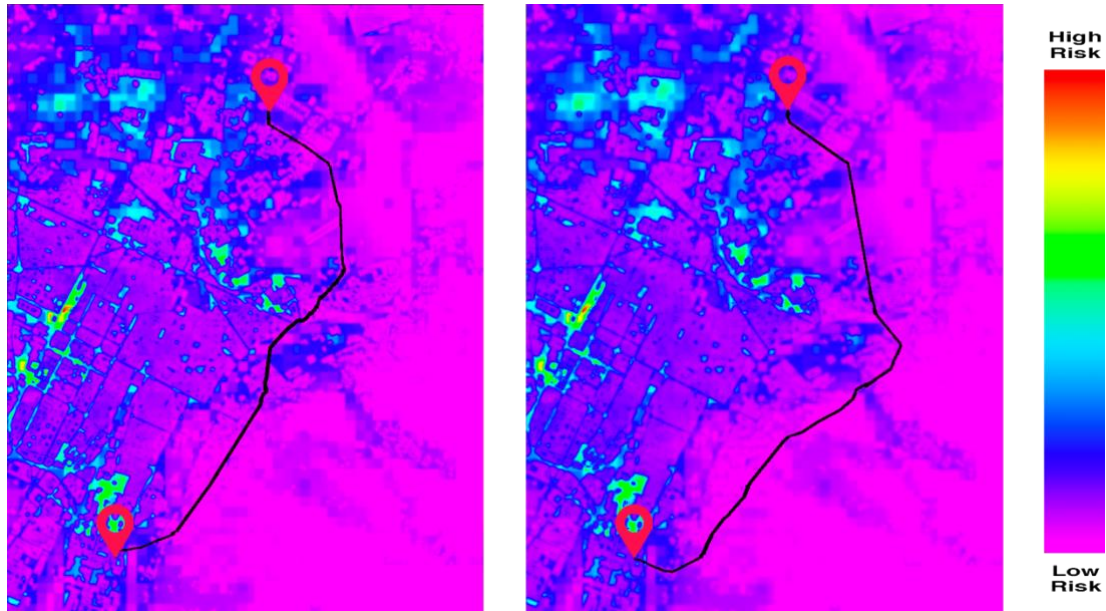


Figure 28 Matrice 200 V2 risk map and optimum trajectory at 20 m of altitude (left) and at 50 m of altitude (right)

3D Visualization

Until now, the simulation has been 2-dimensional. However, the risk-aware path planner also returns the waypoints of each trajectory in GPS coordinates.

Results

Therefore, using Google Earth Studio (29), an online tool provided by Google, it is possible to generate a 3D simulation of the flight. Indeed, knowing the latitude, longitude, and altitude of each waypoint is possible to rebuild the trajectory in a detailed 3-dimensional environment. Moreover, this simulation provides a realistic view of what the pilot could see during the operation.



Figure 29 3D visualization of the simulation of the Matrice 200 V2

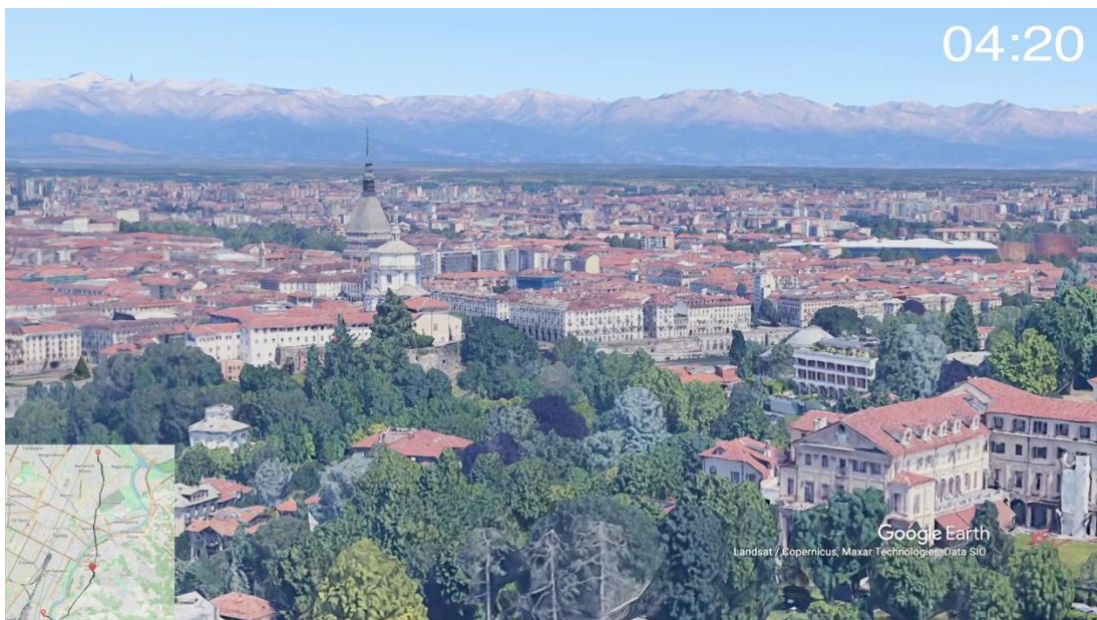


Figure 30 3D visualization of the simulation of the Phantom 4 RTK

This 3D visualization of the trajectory has been done for the Phantom 4 RTK and the Matrice 200 V2. Indeed, they represent the best options for their category. Also, already written above, the fixed-wing cluster is not considered adequate to operate. Thus, in the pictures above, it is possible to see some

screenshots of the result. The entire video simulation could be found on YouTube at the following links.

- **Matrice 200 V2.** <https://youtu.be/XDn1qmwgW5w>
- **Phantom 4 RTK.** <https://youtu.be/yFTMX9DNiY>

Above-the-River Solution

The main limitation of the simulation algorithm is the fixed altitude of the flight. Two simulations, one at 50 *m* and the other at 20 *m* of altitude, have been performed. However, in none of them, a trajectory that follows the Po river emerges. The reason for it lies in the fixed altitude setup. Indeed, flying over a river could be safer as long as the altitude is very low.

Considering that the minimum width of the Po river in the area in question is about 70 meters, the altitude must be around 10 *m* to be sure the UAV will crash upon the river in case of a failure. Hence, this value is too low to perform a full simulation with the algorithm used until now. In fact, the obstacles layer *O* would tag most of the cells of the grid as no-fly zones due to the height of the buildings.

This whole study is crucial since flying directly over the river could probably make getting the authorizations required for the operation from ENAC easier. Hence, this ad hoc solution aims to show the theoretical path length and overall duration of the flight. For the definition of the trajectory, a few assumptions have been made.

The first one regards the approach to the river Po. The starting point, *Ospedale Molinette*, is close to the river; hence, the assumption is that the drone will go straight towards the river.

The second assumption concerns the flight over the river. The UAV will fly at 10 meters above the water surface. In the case of a bridge, the drone will progressively gain altitude, up to 20 *m* from the bridge pavement, before crossing it. Then, it will decrease its altitude to reach 10 *m*. It will proceed approximately until the river Po encounters the river Stura di Lanzo.

At this point, the UAV will make a 90 degrees turn in order to point toward the ending point, *Ospedale San Giovanni Bosco*. The last assumption takes place for this last part. Looking at the map, there are some buildings with more than ten floors in between the route defined. Therefore, an altitude of 50 *m* has been chosen for this last section. Once arrived at the destination, the UAV will land as usual.

Results

Since the risk assessment is not involved in this simulation, the calculation of the duration of the journey has been done for all UAVs, except the eBee SQ/X due to its inability to take off and land vertically. Concerning the length, it follows the assumptions explained above. Hence, it is the same for all of them, namely 9860 meters.

The 2D visualization of the trajectory is shown in Figure 31.

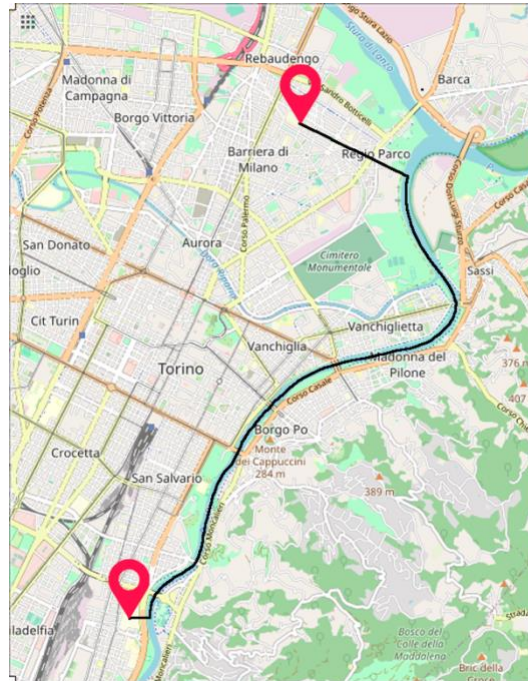


Figure 31 Above-the-river trajectory

Although the first part of the trajectory seems to follow a straighter line to get to the destination, past *Piazza Vittorio Veneto*, in the city center, the river Po heads to the East. Thus, the UAV deviates consistently from the shortest path. Indeed, this wide left turn on the right side of Figure 31 makes this trajectory the longest one among the multirotor UAVs.

The results of this simulation are reported in Table 9. Here, there are the estimations of the duration of the journeys. Since following the river leads to a longer trajectory, the flights also require more time to be completed. The Falcon x8 is less affected by this trajectory. Indeed, its total flight time differs by 0,5 %. Remaining in the same family, the Matrice 200 also shows a slight increase.

Looking at the smaller class, conversely, they suffer a more marked increase in the flight time. For Mavic 2 and Phantom 4, the rise reaches 18 %. The reason behind it lies in the consistently different path they must follow, in comparison to the previous case. Indeed, recalling the explanation of Figure 23 and Figure 24, the fact that these two drones fly closely over the central high-risk area,

Results

represented by three green spots in the middle of the figures, represents a shortcut. Therefore, following the river nullifies this advantage.

	Duration of FF [s]	Total Duration [s]	Variation from fix- altitude at 50 m
Evo II	783	801	+7,8 %
Falcon x8	939	966	+0,5 %
Matrice 200 v2	640	669	+4,5 %
Mavic 2	783	809	+18,2 %
Phantom 4 RTK	704	725	+18,5 %
Wingtra One	880	939	+13,0 %

Table 9 Above-the-river simulation outcome

Regarding the risk associated with this trajectory, its evaluation has been done for the best UAV option of each category, the Phantom 4 RTK and the Matrice 200 V2. This evaluation considers two fixed flight altitudes (20 and 50 meters) above the river. As explained before, this aspect represents a limitation of the algorithm. However, it is interesting the comparison to the average risk and cost of this trajectory, which can be found in Table 10.

	Altitude	Avg risk [$1/h$]	Avg risk variation	Trajectory cost	T. cost variation
Phantom 4 RTK	20 m	$1,735 \cdot 10^{-6}$	-7,7%	$1,221 \cdot 10^{-3}$	+0,9%
	50 m	$1,894 \cdot 10^{-6}$	+9,4%	$1,332 \cdot 10^{-3}$	+30,2%
Matrice 200 V2	20 m	$9,943 \cdot 10^{-6}$	+26,3%	$6,363 \cdot 10^{-3}$	+45,8%
	50 m	$1,120 \cdot 10^{-5}$	+52,6%	$7,167 \cdot 10^{-3}$	+59,5%

Table 10 Above-the-river simulation - average risk and trajectory cost

Results

The result shows how, having considered the same fixed altitudes as the simulations before, the average risk and trajectory cost are higher than those obtained with the optimal path planner. The only simulation that differs from the others is the one regarding the Phantom 4 RTK at 20 meters of altitude. In this case, the river path has a lower average risk, but having larger path length makes the trajectory cost higher than the optimal path at 20 m.

As said above, the main limitation of the algorithm consists of working at a fixed altitude. In order to make this path safer, which means an easier procedure to obtain the authorization from ENAC, a variable altitude is required. The path remains the same, but the altitude varies following the assumptions written at the beginning of this section. Unfortunately, the evaluation of the risk cannot be performed using the current algorithm. However, a visual representation of this simulation at a variable altitude is provided.

In Figure 32, the screenshot of the 3D visualization of this trajectory is shown. Its realization follows the same procedure already explained in the section before. Moreover, the whole simulation, which has been done considering the Matrice 200 V2, can be retrieved at the following link.

- **Matrice 200 V2 – River Po Path.** [https://youtu.be/ BdbWr9foHE](https://youtu.be/BdbWr9foHE)

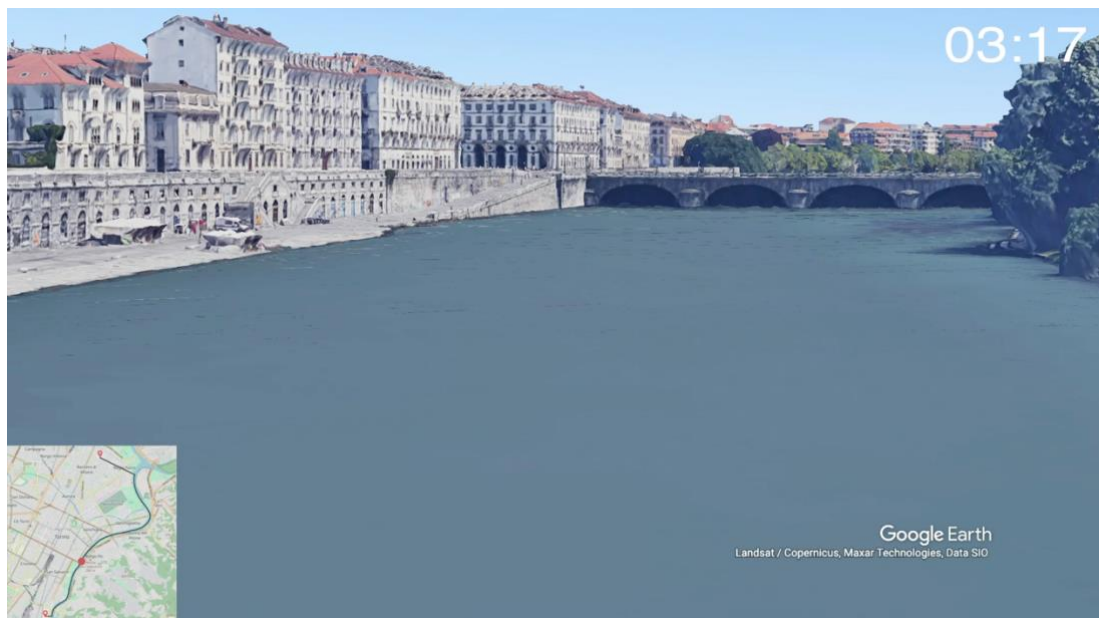


Figure 32 3D visualization of the above-the-river simulation of the Matrice 200 V2

Comparison to Conventional Inter-Hospital Transportation

This entire project aims to find an innovative way to deliver certain kinds of medicines in emergency situations. Therefore, a comparison to today's ways to do it is required. Nowadays, the standard transportation between hospitals consists of sending an ambulance or a car, which is affected by traffic. On average, it takes around 20 minutes to get from *Ospedale Molinette* to *Ospedale San Giovanni Bosco*.

Although the ambulance has priority over regular cars, it also can be involved in an incident while driving to reach the destination. A comparative study conducted in the US by Watanabe et al. (30) showed that an ambulance with warning lights and sirens on is likely involved in 17.1 crashes over 100,000 patient transports. Hence, it means $1,026 \cdot 10^{-3}$ crashes per hour, considering the average transport of 20 minutes. Moreover, in emergency situations, the area around hospitals is congested due to the high request for medical assistance. Therefore, for smaller deliveries, such as life-saving antidotes or blood units, a different solution can be taken into account to support emergency transportation.

Furthermore, healthcare personnel is directly involved in transportation. Regarding either road and air transport, a driver or remote pilot is required. However, looking at recent developments, autonomous flights could take place on settled routes. Therefore, looking at the future, healthcare professionals could just set the UAV up for the flight, and it would reach the destinations autonomously (31). It would be possible to redirect healthcare personnel to other mansions, being more efficient in dealing with emergency situations.

Conclusion

In this master's thesis, several aspects of the transportation of medicines using drones have been addressed. The project aims to analyze an innovative solution to support conventional medical supply. This analysis started with the research of small and mid-size drones available on the market. This step helped to identify the actual technology implemented in the UAV world.

Together with the two stakeholders involved in this project, *ASL Città di Torino* and *Città della Salute e della Scienza di Torino*, a definition of the possible missions has been done. Unfortunately, a quick solution could not be found for all of them. In particular, the main restrictions to some of the missions identified were the European and Italian regulations. This last aspect plays a crucial role throughout the whole thesis. Indeed, regulations are evolving continuously in order to follow the market progress. Moreover, a different way of comparing different drones has been done through the principal components analysis. By utilizing statistical learning techniques, it was possible to cluster the drones found by their performances and dimensions.

Lastly, the risk assessment and the procedure to optimize the route contribute to the generation of the risk maps and optimal trajectory to link the two hospitals considered. Those two are peculiar for each drone and represent a part of the decision making to choose the best drone possible once given the operation to be completed.

The outcome of the whole project shows that UAVs have great potential in the healthcare sector. Their ability to reach every location quickly while avoiding traffic congestions makes them crucial support to decision-makers. Indeed, in the simulation run in this project, linking the two hospitals considered by any drone takes less time than conventional road transport.

Looking at the wider picture, transportation outside urban areas could also benefit from the implementation of this technology. In the case of an emergency, roads could suffer damages; therefore, the time to get to the destination could be consistently high. UAVs have the capabilities to reach isolated areas in a short time. Moreover, looking at recent developments, drones are expected to be more and more autonomous (31), meaning that the professionals involved in the emergency could take care of more critical issues than dealing with the actual transportation of goods.

However, drones cannot replace the current medical transportation system completely. Indeed, bad weather, payload limitations, and the regulatory

Conclusion

framework are the main constraints to their implementation. These aspects are still critical to have a safe and guaranteed delivery of any good under any circumstance. For these reasons, UAVs are expected to support, rather than replace, the current delivery of medical goods. In particular, several studies have been done to prove their feasibility on the last-mile delivery (32).

In conclusion, recent developments in UAV technology demonstrate the possible application of drones in any field, in particular in the healthcare sector. Several problems of different nature need to be solved yet, but their great potential indicates that more and more drones are expected to fly for a variety of scopes. Therefore, this work could be seen as a preliminary study on their applicability in an urban context, such as the city of Torino, and as the first step towards the creation of an airlink between two major hospitals of the city.

Bibliography

1. Hii, M.S.Y., Courtney, P. and Royall, P.G. An Evaluation of the Delivery of Medicines Using Drones. *Drones*. 2019, Vol. 3, 52.
2. Thiels, C., et al. Use of Unmanned Aerial Vehicles for Medical Product Transport. *Journal of Air Medical Transport*. 2015, Vol. 34, 2.
3. Osservatorio Droni. *Droni: pronti al decollo!* s.l. : Politecnico di Milano, 2020.
4. De Miguel Molina, B. and Segarra Oña, M. The Drone Sector in Europe. [book auth.] M. De Miguel Molina and V. Santamarina Campos. *Ethics and Civil Drones*. s.l. : SpringerBriefs in Law, 2018.
5. Cestino, E. and Romeo, G. Innovative Unmanned Aircrafts: role and constraints for GMES applications. *3rd CEAS Air & Space Conference*. 2011.
6. Amukele, T., et al. Drone transportation of blood products. *Transfusion*. 2016, Vol. 57.
7. Eichleay, M., et al. Using the Unmanned Aerial Vehicle Delivery Decision Tool to Consider Transporting Medical Supplies via Drone. *Glob Health Sci Pract*. 2019, Vol. 7, 4, pp. 500-506.
8. Palmer, A. Amazon wins FAA approval for Prime Air drone delivery fleet. *CNBC*. [Online] August 31, 2020. <https://www.cnbc.com/2020/08/31/amazon-prime-now-drone-delivery-fleet-gets-faa-approval.html>.
9. Google Maps Platform. *Google*. [Online] <https://cloud.google.com/maps-platform>.
10. Regolamento ENAC, Mezzi Aerei a Pilotaggio Remoto, Ed.3, Emendamento 1 del 14 luglio 2020.
11. James, G., et al. *An Introduction to Statistical Learning with Applications in R*. New York : Springer, 2013. ISBN 978-1-4614-7137-0.
12. Welcome to Python.org. *Python*. [Online] <https://www.python.org>.
13. scikit-learn: machine learning in Python. *scikit-learn*. [Online] <https://scikit-learn.org/stable/#>.

Bibliography

14. aperTO - Gli Open Data della Città di Torino. *aperTO*. [Online] <http://aperto.comune.torino.it>.
15. Commission Delegated Regulation (EU) 2019/945 of 12 March 2019 on unmanned aircraft systems and on third-country operators of unmanned aircraft systems.
16. Commission Implementing Regulation (EU) 2019/947 of 24 May 2019 on the rules and procedures for the operation of unmanned aircraft.
17. D-Flight - Enabling Autonomous Flight. *D-Flight*. [Online] <https://www.d-flight.it/portal/>.
18. Circolare ENAC ATM-09, Aeromobili a pilotaggio remoto - Criteri di utilizzo dello spazio aereo del 24 maggio 2019.
19. Hwang, M.-H., Cha, H.-R. and Jung, S.Y. Practical Endurance Estimation for Minimizing Energy Consumption of Multirotor Unmanned Aerial Vehicles. *Energies*. 2018, Vol. 11, 2221.
20. Primatesta, Stefano, et al. An Innovative Algorithm to Estimate Risk Optimum Path for Unmanned Aerial Vehicles in Urban Environments. *Transportation Research Procedia*. 2018, Vol. 35, pp. 44-53.
21. Primatesta, S., Rizzo, A. and Ia Cour-Harbo, A. Ground Risk Map for Unmanned Aircraft in Urban Environments. *Journal of Intelligent & Robotic Systems*. 2020, Vol. 97, pp. 489–509.
22. Condizioni meteorologiche medie a Torino. *Weather Spark*. [Online] <https://it.weatherspark.com/y/55583/Condizioni-meteorologiche-medie-a-Torino-Italia-tutto-1%27anno>.
23. OpenStreetMap. *OpenStreetMap*. [Online] <https://www.openstreetmap.org/>.
24. Rapporto URBES 2015. *Istat*. [Online] <https://www.istat.it/storage/urbes2015/torino.pdf>.
25. Guglieri, G., Quagliotti, F. and Ristorto, G. Operational issues and assessment of risk for light UAVs. *Journal of Unmanned Vehicle Systems*. 2014, Vol. 2, 4, pp. 119-129.
26. Ia Cour-Harbo, A. Quantifying ground impact fatality rate for small unmanned aircraft. *Journal of Intelligent & Robotic Systems*. 2019, Vol. 93, 1-2, pp. 367–384.

Bibliography

27. Guglieri, G., Lombardi, A. and Ristorto, G. Operation Oriented Path Planning Strategies for Rpas. *American Journal of Science and Technology*. 2015, Vol. 2, 6, pp. 321-328.
28. Metodologia di Valutazione del Rischio in Operazione RPAS per Autorizzazioni e Permessi di Volo Non Geografici - Guida Applicativa. *Linee Guida ENAC*. January 9, 2020, 2017/001-NAV.
29. Google Earth Studio. *Google*. [Online] <https://www.google.com/intl/it/earth/studio/>.
30. Watanabe, B. L., et al. Is Use of Warning Lights and Sirens Associated With Increased Risk of Ambulance Crashes? A Contemporary Analysis Using National EMS Information System (NEMSIS) Data. *Ann Emerg Med*. Jul 2019, Vol. 74, 1, pp. 101-109.
31. Floreano, D. and Wood, R. Science, technology and the future of small autonomous drones. *Nature*. 2015, Vol. 521, pp. 460-466.
32. Aurambout, J-P., Gkoumas, K. and Ciuffo, B. Last mile delivery by drones: an estimation of viable market potential and access to citizens across European cities. *European Transport Research Review*. 2019, Vol. 11.
33. Falcon. *Airborne Drones*. [Online] <https://www.airbornedrones.co/falcon/>.
34. Vanguard. *Airborne Drones*. [Online] <https://www.airbornedrones.co/vanguard/>.
35. Evo II. *Autel Drones*. [Online] <https://auteldrones.com/pages/evo2>.
36. Matrice 200 series. *DJI*. [Online] <https://www.dji.com/it/matrice-200-series-v2/info#specs>.
37. Matrice 600. *DJI*. [Online] <https://www.dji.com/it/matrice600/info#specs>.
38. MG-1P. *DJI*. [Online] <https://www.dji.com/it/mg-1p>.
39. Mavic 2. *DJI*. [Online] <https://www.dji.com/it/mavic-2-enterprise/specs>.
40. Inspire 2. *DJI*. [Online] <https://store.dji.com/it/product/inspire-2?from=search-result-v2&position=0&vid=20221>.
41. Phantom 4 RTK. *DJI*. [Online] <https://www.dji.com/it/phantom-4-rtk/info>.

Bibliography

42. EWG-E3. *Ewatt UAV*. [Online] https://docs.wixstatic.com/ugd/592fc8_43b203a9b6f5438dae35b16b1d8e236c.pdf.
43. ESPECT. *Ewatt UAV*. [Online] <https://www.ewattuav.com/espect>.
44. EWZ-D6. *Ewatt UAV*. [Online] https://docs.wixstatic.com/ugd/592fc8_5c2a44666c3b40c697d6247323a104eb.pdf.
45. EWZ-S8. *Ewatt UAV*. [Online] <https://www.ewattuav.com/ewz-s8-draft>.
46. Alta 8. *Freefly systems*. [Online] <https://freeflysystems.com/alta-8/specs>.
47. Alta X. *Freefly systems*. [Online] <https://freeflysystems.com/alta-x/specs>.
48. Falcon 8. *Intel*. [Online] <https://www.intel.it/content/www/it/it/products/drones/falcon-8.html>.
49. Levante. *Italdron*. [Online] <https://www.italdron.com/levante>.
50. Titan XLE. *Italdron*. [Online] <https://www.italdron.com/droni-professionali-e-accessori/droni-professionali/titan-xle>.
51. Titan LE. *Italdron*. [Online] <https://www.italdron.com/drone-professionale-titan-le>.
52. BIGONE 8HSE. *Italdron*. [Online] <https://www.italdron.com/droni-professionali-e-accessori/droni-professionali/bigone-8hse>.
53. EVO4HSE RTK. *Italdron*. [Online] <https://www.italdron.com/droni-professionali-e-accessori/droni-professionali/4hse-evo>.
54. M2V9. *Swiss Post*. [Online] <https://www.post.ch/en/about-us/innovation/innovations-in-development/drones?shortcut=opp-en-about-us-company-innovation-swiss-post-s-innovations-for-you-drones#use-of-drones>.
55. ATLAS-T. *Nextech*. [Online] <https://shop.airbornedrones.co/products/drone>.
56. ATLAS-V. *Nextech*. [Online] <https://shop.airbornedrones.co/products/vtol-drone>.
57. eBee X. *senseFly*. [Online] <https://www.sensefly.com/drone/ebec-x-fixed-wing-drone/>.

Bibliography

58. eBee SQ. *senseFly*. [Online] <https://www.sensefly.com/drone/ebec-sq-agriculture-drone/>.
59. SF6 VTOL RPV. *Skyrobotic*. [Online] <http://www.skyrobotic.com/wp-content/uploads/2016/07/skyrobotic-brochure-SR-SF6.pdf>.
60. Tarot 650. *UAV System int.* [Online] <https://uavsystemsinternational.com/products/tarot-650-ready-to-fly-drone?variant=29472197836879>.
61. UVM 2E. *UAVOS*. [Online] <https://www.uavos.com/products/vtols/multicopter-uvm-2e>.
62. Heavy Pro. *Valkyrie*. [Online] <https://www.valkyrie.pro/>.
63. DeltaQuad. *Vertical Technologies*. [Online] <https://www.deltaquad.com/vtol-drones/cargo/#specifications>.
64. VideoDrone. *VideoDrone Finland Oy*. [Online] <https://videodrone.fi/en/videodrone/>.
65. WingtraOne. *Wingtra*. [Online] <https://wingtra.b-cdn.net/wp-content/uploads/Wingtra-Technical-Specifications.pdf>.
66. Cinema Serie. *xFold*. [Online] <http://www.xfoldrig.com/xfold-cinema/>.
67. H520. *Yuneec*. [Online] https://www.yuneec.com/it_IT/commerciale/droni/h520/panoramica.html.
68. Typhoon H3. *Yuneec*. [Online] https://www.yuneec.com/it_IT/commerciale/droni/typhoon-h3/panoramica.html.
69. Tornado H920. *Yuneec*. [Online] <https://shop.yuneec.com/eu/camera-drones/tornado-h920/tornado-h920/>.

Appendix A – UAVs Data

Manufacturer	Name	Type	Endurance (min)	Range (km)	Weight (kg)	Dimensions (cm)			Payload max weight (kg)	Cruise speed (m/s)	Max wind (m/s)
						Width	Length	Height			
	Falcon x8 (33)	Rotor	32	18,5	4	53	45	10	2	15	6,9
Airborne Drones	Falcon x4 (33)	Rotor	50	18,5	4	53	45	10	0,5	15	4,1
	Vanguard (34)	Rotor	70	35	9,5	83,5	83,5	35	0,85	18	10,3
Autel Drones	Evo II (35)	Rotor	40	9	1,15	39,7	39,7	-	-	20	17
	Matrice 200 V2 (36)	Rotor	26	8	4,69	88,3	88,6	39,8	1,45	17	12
	Matrice 600 (37)	Rotor	30	5	9,6	168,8	151,8	-	6	18	8
DJI	MG-1P (38)	Rotor	20	-	13,7	150	150	57,8	10	10	8
	Mavic 2 (39)	Rotor	31	8	0,9	32,2	24,2	8,4	0,2	20	9,7
	Inspire 2 (40)	Rotor	23	7	4,25	42,5	42,7	31,7	0,81	26,1	10
	Phantom 4 RTK (41)	Rotor	30	7	1,4	35	35	20	-	20	-

Manufacturer	Name	Type	Endurance (min)	Range (km)	Weight (kg)	Dimensions (cm)			Cruise speed (m/s)	Max wind (m/s)	
						Width	Length	Height			
Ewatt Aerospace	EWG-E3 (42)	Rotor + wing	80	-	9,5	300	200	35	2	18	10
	ESPECT (43)	Rotor	29	-	3,2	-	-	-	0,8	15	-
	EWZ-D6 (44)	Rotor	35	-	14,3	170	170	55	5	12	10
	EWZ-S8 (45)	Rotor	34	-	9,8	113	113	52	5	20	8
Freefly	Alta 8 (46)	Rotor	25	-	6,2	132,5	132,5	26,3	9,1	-	-
	Alta X (47)	Rotor	41,7	-	10,4	227,3	227,3	38,7	15,9	-	-
Intel	Drone Intel® Falcon™ 8+ (48)	Rotor	26	-	2	76,8	81,7	16	0,81	18	-
	Levante (49)	Rotor	60	1,5	5	100	100	38	1	8	12
Italdron	Titan XLE (50)	Rotor	15	1,5	5	88	88	33	1	5	13
	Titan LE (51)	Rotor	18	1,5	4,5	57	57	33	1	10	13
	BIGONE 8HSE (52)	Rotor	45	1,5	13	128	128	60	10	10	13
	EVO4HSE RTK (53)	Rotor	15	1,5	6,5	63	63	43	2,5	10	13

Manufacturer	Name	Type	Endurance (min)	Range (km)	Weight (kg)	Dimensions (cm)			Payload max weight (kg)	Cruise speed (m/s)	Max wind (m/s)
						Width	Length	Height			
Matternet Inc.	M2V9 (54)	Rotor	-	20	11,2	80	80	20	2	16	-
Nextech	ATLAS-T (55)	Rotor	80	20	15	110,6	110,6	17,6	-	18	12,5
	ATLAS-V (56)	Rotor	180	100	9	320	-	-	3	27,7	-
senseFly	eBee X (57)	Wing	90	8	1,1	116	-	-	0,3	30	12,8
	eBee SQ (58)	Wing	55	8	1,1	110	-	-	-	30	12
Skyrobotic	SF6 VTOL RPV (59)	Rotor	39	-	2,25	110	110	36	2	-	-
UAV System int.	Tarot 650 (60)	Rotor	25	3,2	2,18	-	-	-	1,5	15	-
UAVOS	UVM 2E (61)	Rotor	55	10	-	162	162	51	1	15,3	-
Valkyrie	Heavy Pro (62)	Rotor	-	20	7,6	-	-	-	30	25	-
Vertical Technologies	DeltaQuad Pro #CARGO (63)	Rotor + wing	110	100	5	235	90	-	1,2	16	-

Manufacturer	Name	Type	Endurance (min)	Range (km)	Weight (kg)	Dimensions (cm)			Cruise speed (m/s)	Max wind (m/s)	
						Width	Length	Height			
VideoDrone Finalnd Oy	Videodrone (64)	Rotor	35	-	2	58	58	37	4,4	15	15
Wingtra	WingtraOne (65)	Wing	59	10	3,7	125	68	12	0,8	16	8
xFold	Cinema Serie (66)	Rotor	24	-	6,5	96,5	106,7	62,2	11,3	-	-
	H520 (67)	Rotor	25	1,6	1,633	52	45,5	29,5	-	-	-
Yuneec	Typhoon H3 (68)	Rotor	25	1,6	2	52	52	-	-	20	-
	Tornado H920 (69)	Rotor	24	1,6	5	92	92	-	-	11	-

Appendix B – Centro Anti Veleni

Principio attivo	Forma farmaceutica	Indicazione all' uso	Via di somministrazione	Posologia	Conservazione
Alcool Etilico 95°-96°	Soluzione iniettabile Fiale da 2-10ml	Alcoli - Glicoli (es. metanolo, glicole etilenico)	Endovenosa	Solitamente si utilizza la diluizione di 5 fl in 500 cc di fisiologica da infondere a 10 ml/kg in 40 min e successiva infusione di mantenimento a 2 ml/kg/h monitorando l' etanolemia ogni 2 ore.	A temperatura ambiente, lontano da fiamma o da altra sorgente di calore.
Amile nitrito	Soluzione inalatoria Fiale da 1ml	Cianuri da utilizzare in fase extraospedaliera e nelle grandi emergenze.	Inalatoria	Rompere 1-2 fiale su garza e far inalare per 30 sec ogni minuto per 3 minuti. Il trattamento è ripetibile fino a inizio di somministrazione di altri antidoti per via endovenosa. Non superare una metaHb del 30%.	A temperatura ambiente.
Atropina Solfato	Soluzione iniettabile Fiale da 0,5-1mg/ml	Carbamati esteri organo fosforici agenti nervini ipertono colinergico (funghi del genere Clitocybe e Inocybe)	Endovenosa	Boli da 1mg fino a scomparsa della broncorrea e delle secrezioni da ipertono colinergico. Possibilità di infusione continua da concordare con lo specialista del CAV.	A temperatura ambiente. Proteggere dalla luce.
Bicarbonato di Sodio	Soluzione perfusionale 8,4% Fiale da 10ml Fiaconi da 100-250-500ml	Alcalinizzazione di plasma e urine Cardiotossicità da farmaci (es. chinidina, antidepressivi triciclici) Aumento escrezione urinaria di alcuni farmaci (es. fenobarbitale, ac. Acetilsalicilico)	Endovenosa	La dose dipende dall'età, dal peso e dalle condizioni cliniche del paziente. Nelle forme subacute e croniche di acidosi metabolica somministrare da 2 a 5 mEq di bicarbonato per kg di peso durante 4-8 ore. Nei bambini, in caso di necessità, somministrare molto lentamente e non più di 8 mEq/kg di peso corporeo per evitare diminuzione della pressione cerebrospinale e possibili emorragie intracraniche.	Conservare a temperatura non superiore a 30°C.
Blu di metilene (metitioninio cloruro)	Soluzione iniettabile 1% Fiale da 100mg/10ml	Sostanze metaemoglobinizzanti oppure shock distributivo o neurotossicità da Ifosfamide	Endovenosa	1-2mg/kg in 5 minuti. La ripetizione della somministrazione dipende dall'indicazione d'uso. Non superare i 7mg/kg in 24 ore.	Temperatura ambiente ed al riparo della luce.

Principio attivo	Forma farmaceutica	Indicazione all' uso	Via di somministrazione	Posologia	Conservazione
Calcio cloruro diidrato	Soluzione iniettabile fiale da 10ml al 10%	Ipocalcemie gravi per ingestione di fluoruri e ossalati (es. antiruggine)	Endovenosa (tramite catetere venoso centrale)	1 fiala diluita in 100ml di soluzione fisiologica in 5-10 minuti, seguita da mantenimento da concordare con lo specialista del CAV.	A temperatura ambiente.
Calcio gluconato	Soluzione iniettabile fiale da 10ml al 10%	Ipocalcemie per ingestione di fluoruri e ossalati (es. antiruggine) Contatto cutaneo con fluoruri e ossalati (es. antiruggine)	Endovenosa (periferica) o Orale (per ingestione di fluoruri o ossalati) o Uso topico per contatti cutanei	2-3 fiale in 5-10 minuti, seguita da mantenimento 1-2gr per via orale per applicazioni cutanee in mancanza di "calcium gel"	A temperatura ambiente.
Carbone vegetale attivato in polvere	Polvere per sospensione orale Flacone da 50g	Utile nell' adsorbimento di sostanze tossiche ingerite, in modo da ridurre l' assorbimento sistemico, rendendole meno disponibili e facilitandone l' eliminazione. Può essere usato dopo l' induzione di emesi o dopo la lavanda gastrica ed anche insieme all' emodialisi.	Orale	0,5-1 g/kg. Possibili somministrazioni ripetute. 2-5 g/ora se necessaria dialisi gastrointestinale. Da somministrare il più precocemente possibile in dosi 10 volte maggiori alla dose di sostanza tossica assunta.	Temperatura ambiente e al riparo dell' umidità.
Dantrolene sale sodico	Polvere liofilizzata Flacone da 20mg	Ipertermia maligna	Endovenosa	1-2 mg/kg rapidamente, ripetibile fino a un max di 10 mg/kg.	Non conservare a temperatura superiore ai 25°C. Dopo la preparazione, conservare la soluzione al riparo dalla luce diretta. Non conservare la soluzione a temperatura inferiore a 15 °C e superiore a 25 °C.

Principio attivo	Forma farmaceutica	Indicazione all'uso	Via di somministrazione	Posologia	Conservazione
Dexrazoxano cloridrato	Polvere per preparazioni iniettabili Flaconcini da 500mg	Stravaso di antraciline Prevenzione tossicità da antraciline	Endovenosa	La dose raccomandata, per il primo giorno, è 1.000 mg/m ² . Seguita da altri 1000 mg/m ² il secondo giorno e da 500 mg/m ² il terzo giorno.	Conservare a temperatura inferiore a 25 °C, al riparo dalla luce.
Diazepam	Soluzione iniettabile Fiale da 10mg/2ml	Intossicazione da esteri organofosforici Intossicazione da cloroquina Uso sintomatico nel trattamento di stati di agitazione, di eccitazione motoria di eziologia diversa, nei quadri clinici paranoici-allucinatori, nello stato di male epilettico, spasmi muscolari, nel tetano, in caso di convulsioni febbrili del lattante e del bambino e nella sindrome extrapiramidale indotta da altre sostanze.	Endovenosa	Adulti: 2 mg/kg in bolo da 30 minuti (con adeguata assistenza respiratoria) seguito da 1-2 mg/kg nelle 24 ore. Bambini: 0,2-0,5 mg /Kg endovena ogni 5 minuti secondo necessità; può essere somministrato anche per via rettale.	A temperatura ambiente non superiore ai 30°C.
Dimetilsulfossido - DMSO 99%	Preparato galenico	Stravaso di antraciline e antibiotici non antracilici (es. mitomicina)	Topica	Applicazioni topiche di 1-2ml su un'area di dimensioni doppie rispetto a quella interessata dall'infiltrazione, ogni 2 ore per le prime 24 ore.	Conservare in luogo asciutto, a temperatura inferiore a 25°C ed al riparo dalla luce.
Emulsioni lipidiche 20%	Soluzione infusione Sacca da 100-250-500-1000 ml	Cardiotossicità refrattaria da agenti liposolubili, anestetici, farmaci cardioattivi.	Endovenosa	Bolo iniziale da 1,5 ml/kg seguito da infusione continua 0,25-0,5 ml/kg/min	Conservare a temperatura inferiore 25°C senza mai congelare.
Fisostigmina salicilato	Soluzione iniettabile fiale da 1mg/ml, 2mg/5ml, 2mg/2ml.	Sindrome anticolinergica centrale	Endovenosa	La dose iniziale è di 0,5-1,2 mg (2 mg) può essere seguita da una seconda dose nel caso in cui non si osservi nessuna risposta entro 30 minuti.	In contenitori ben chiusi al riparo dalla luce. Il medicinale non richiede particolari condizioni di conservazione relativamente alla temperatura.

Principio attivo	Forma farmaceutica	Indicazione all' uso	Via di somministrazione	Posologia	Conservazione
Flumazenil	Soluzione iniettabile Fiale da 0,5mg/5ml o 1mg/10ml	Intossicazione da benzodiazepine e ipnotici non benzodiazepinici.	Endovenosa	Adulti: 0,3 mg endovena ripetibile; infusione continua di 0,5-1 mg/h secondo necessità clinica. Bambini: 0,01 mg/Kg endovena ripetibili.	A temperatura ambiente e al riparo dalla luce.
Frammenti anticorpali antidigitale	Polvere liofilizzata, frammenti anticorpali (Fab) di origine ovina Flacone da 40mg	Intossicazioni gravi da glicosidi digitalici (digossina, derivati della digossina e digitossina)	Endovenosa	Dose da calcolare in rapporto alla digossinemia o ai mg di glucoside assunto in sovradosaggio. Se non è possibile stimare la dose ingerita o determinare la digossinemia e si è certi della diagnosi si possono somministrare 1-3 fiale ripetibili entro 60 minuti se non vi è risposta clinica.	Temperatura tra i 2° e gli 8° C.
Glucagone cloridrato	Polvere e solvente per soluzione iniettabile Flacone da 1mg + fiala 1ml	Intossicazioni da beta-bloccanti con scarsa o nessuna risposta all' atropina.	Endovenosa	Adulti: 5-10 mg endovena seguito da 1-10 mg/h. Bambini: 0,15 mg/Kg endovena seguito da 0,05-0,1 mg/Kg/h.	A temperatura compresa tra i 2° e gli 8°C, non congelare.
Ialuronidasi	Polvere per preparazione iniettabile Fiala da 1500 IU/1ml	Stravasato di etoposide, alcaloidi della vinca e taxani.	Sottocutanea	Stabilita dal medico prescrittore a seconda dell' entità dei versamenti.	Conservare ad una temperatura non superiore ai 25°C.
Idarucizumab	Soluzione iniettabile Flaconcino da 2,5g/50ml	Inattivatore specifico per dabigatran ed è indicato nei pazienti adulti trattati con Pradaxa (dabigatran etexilato) nei casi in cui si rende necessaria l' inattivazione rapida dei suoi effetti anticoagulanti: negli interventi chirurgici di emergenza/nelle procedure urgenti; nel sanguinamento potenzialmente fatale o non controllato.	Endovenosa	5 g (2 x 2,5 g/50 mL)	Temperatura tra i 2° e gli 8° C.

Principio attivo	Forma farmaceutica	Indicazione all' uso	Via di somministrazione	Posologia	Conservazione
Idrossicobalamina	Polvere liofilizzata Flacone da 5g	Avvelenamento da cianuri, in associazione con sodio tiosolfato.	Endovenosa	Dose iniziale pari a 5 g, somministrata mediante infusione endovenosa della durata di 15 minuti.	Temperatura tra i 2° e gli 8° C.
Ioduro di potassio	Preparato galenico	Iodio radioattivo	Orale	Adulti: 130mg/die. Bambini: 65mg/die. Neonati: 16mg/die.	Temperatura di stoccaggio consigliata: 15 – 25 °C.
Ipecacuana sciroppo emetico	Sciroppo Flacone 14ml al 7% Flacone 30ml al 7%	Induzione dell'emese	Orale	Adulti: 30 ml di sciroppo al 7% seguito da 250-500 ml di acqua. Bambini fino a 1-12 anni di età: 10-15 ml di sciroppo al 7% seguito da 150-250 ml di acqua. Neonati da 1 a 12 mesi: 5-1 ml di sciroppo seguito da 10-20 ml/Kg di acqua.	A temperatura inferiore ai 25°C.
Magnesio solfato polvere	Polvere per sospensione Buste da 30g	Catartico Ingestione di Bario	Orale	10-30g nell'adulto. L'effetto può comparire tra i 30 minuti e le 6 ore.	Temperatura ambiente in confezionamento integro, in contenitori ben chiusi e al riparo dalla luce e dal calore.
Mannitolo	Soluzione per infusione 5% - 10% 18% - 20%	Intossicazione da ciguatera (cioè la ciguatera, che è la forma più comune di intossicazione da pesce) e grave tossicità da vitamina A	Endovenosa	0,25-1g/kg in 30-45 minuti	Tenere a temperatura ambiente perché a freddo cristallizza.
Naloxone cloridrato	Soluzione iniettabile Fiala da 0,4mg/ml	Intossicazione da oppioidi.	Endovenosa Intramuscolare Sottocutanea Inalatoria per aerosol Endonasale con device	0,4-4mg in bolo. Possibili somministrazioni ripetute o infusione continua.	A temperatura ambiente e al riparo dalla luce.

Principio attivo	Forma farmaceutica	Indicazione all' uso	Via di somministrazione	Posologia	Conservazione
Paraffina liquida - olio di vaselina	Emulsione orale Flacone da 200ml	Intossicazione da derivati del petrolio e solventi.	Orale	Adulti: 15-45 ml Bambini di età compresa tra 2 e 12 anni: 5-15 ml	Al di sotto dei 30°C
Polietilenglicole 400 (PEG 400, MACROGOL 400)	Flaconi da 500ml o 1000ml	Decontaminazione cutanea da fenoli	Uso topico	Quantità necessaria in rapporto alla superficie dell'area da decontaminare-	A temperatura ambiente, al riparo dalla luce, in contenitori non permeabili all' aria.
Polietilenglicole 3350/4000 (PEG, MACROGOL)	Polvere per soluzione orale Polvere per sospensione addizionata di elettroliti	Catarsi Lavaggio intestinale	Orale Gastrica via sondino	Moviprep: 2 bustine A + 2 bustine B in 2L di acqua. Selg/Selg-esse: 35-70g in una somministrazione.	A temperatura ambiente, al riparo dalla luce, in contenitori non permeabili all' aria.
Protamina Cloridrato	Soluzione iniettabile Fiala 50mg/5ml	Sovradosaggio da eparina.	Endovenosa	Adulti: 1 mg di protamina cloridrato o solfato ogni 100 U.I. di eparina, in infusione endovenosa lenta, fino a 50 mg in 10 minuti. Se l' emorragia non si arresta entro 15 minuti si deve somministrare il contenuto di una seconda fiala e continuare la somministrazione finchè il tempo di protrombina non si sia normalizzato	A temperatura non superiore a 25°C
Simeticone	Gocce orali - sospensione Flacone da 30ml al 6,66%	Intossicazione da sostanze schiumogene (es. saponi, shampoo...)	Orale	Adulti: 100-500 mg in gocce per os. Bambini: 40-80 mg in gocce per os.	A temperatura ambiente, al riparo da luce e umidità.

Principio attivo	Forma farmaceutica	Indicazione all' uso	Via di somministrazione	Posologia	Conservazione
Sodio Tiosolfato (iposolfito di sodio)	Soluzione iniettabile Fiala da 1g/10ml	Ingestione di ipoclorito di sodio (candeggina classica, varechina). Intossicazione da cianuri. Stravaso di mecloretamina, oxaliplatino, cisplatino e carboplatino.	Orale Endovenosa Sottocutanea	Adulti: 10 gr di tiosolfato in 250 ml di soluzione fisiologica o glucosata al 5%, endovena, in 30 minuti; contemporanea infusione di idrossocobalamina 5 gr in 250 ml di soluzione fisiologica o glucosata al 5%; entrambi eventualmente ripetibili.	A temperatura ambiente (tra 15° e 30°C) al riparo dalla luce, nei contenitori ermeticamente chiusi. Non congelare.
Terra di Fuller	Polvere per sospensione Barattolo da 60g	Paraquat e diquat (diserbanti)	Orale	Sospensione al 15% di 100 g di farmaco per os, seguita da 3 dosi successive di 50 g ogni 2 ore.	A temperatura non superiore ai 30 °C; le confezioni sigillate non hanno scadenza.
Vitamina B6 - piridossina cloridrato	Soluzione iniettabile Fiale da 300mg/2ml	Intossicazioni da isoniazide e da idrazina; altre possibili applicazioni: intossicazione da glicole etilenico e funghi del genere Gyromita.	Endovenosa	Fino ad un massimo di 20g al giorno.	A temperatura ambiente ed al riparo dalla luce
Vitamina K - fitomenadione	Soluzione iniettabile Fiala da 10mg/ml	Ipotrombinaemia conseguente ad intossicazione da salicilati.	Endovenosa Intramuscolare Orale	5-10mg fino a 10-50mg da 2 a 4 volte al giorno.	Non conservare a temperatura superiore a 25° C; non congelare

Appendix C – UAVs’ PCA Scores

	Principal Component 1	Principal component 2	Principal component 3
Falcon x4	-1,91	1,50	2,16
Falcon x8	-1,92	0,92	1,59
Vanguard	0,27	0,69	-0,05
Evo II	-2,33	0,65	0,04
Inspire 2	-1,60	0,66	0,62
Matrice 200 V2	-0,96	0,86	-0,01
Matrice 600	1,14	-1,05	1,29
Mavic 2	-2,83	1,31	0,78
MG-1P	1,34	-2,39	1,23
Phantom 4 RTK	-2,05	0,45	0,33
ESPECT	-1,57	0,50	-0,01
EWG-E3	3,55	1,36	0,46
EWZ-D6	2,12	-1,65	-0,07
EWZ-S8	1,17	-0,10	1,09
Alta 8	0,68	-0,48	0,59
Alta X	3,38	-1,24	1,15

Appendix C

	Principal Component 1	Principal component 2	Principal component 3
Drone Intel® Falcon™ 8+	-0,63	-0,45	-0,68
BIGONE 8HSE	1,51	-2,45	-1,23
EVO4HSE RTK	-1,16	-1,38	-1,48
Levante	-0,59	-0,67	-1,28
Titan LE	-1,78	-0,95	-1,35
Titan XLE	-1,37	-1,53	-1,53
M2V9	-0,51	-0,23	-0,01
ATLAS-T	1,14	0,21	-0,92
ATLAS-V	5,81	3,89	-0,90
eBee SQ	-0,38	1,48	-0,19
eBee X	0,08	1,98	-0,41
SF6 VTOL RPV	-0,70	-0,53	-0,70
Tarot 650	-1,81	-0,11	0,18
UVM 2E	3,53	-1,04	-1,82
Heavy Pro	2,12	-2,50	3,05
DeltaQuad Pro #CARGO	2,26	2,88	-0,26
Videodrone	-0,83	-0,15	-1,76
WingtraOne	-0,57	1,42	0,10

Appendix C

	Principal Component 1	Principal component 2	Principal component 3
Cinema Serie	1,26	-1,23	0,22
H520	-2,23	-0,07	-0,07
Tornado H920	-1,08	-0,91	-0,09
Typhoon H3	-2,56	0,36	-0,04